



University of Kentucky  
UKnowledge

---

Theses and Dissertations--Biomedical  
Engineering

Biomedical Engineering

---


2018

## SYNTHESIS AND CHARACTERIZATION OF BLUE LIGHT POLY( $\beta$ -AMINO ESTER)S

Nicholas John Kohrs

University of Kentucky, [nkohrs83@gmail.com](mailto:nkohrs83@gmail.com)

Author ORCID Identifier:

 <https://orcid.org/0000-0002-4397-0459>

Digital Object Identifier: <https://doi.org/10.13023/etd.2018.406>

[Right click to open a feedback form in a new tab to let us know how this document benefits you.](#)

---

### Recommended Citation

Kohrs, Nicholas John, "SYNTHESIS AND CHARACTERIZATION OF BLUE LIGHT POLY( $\beta$ -AMINO ESTER)S" (2018). *Theses and Dissertations--Biomedical Engineering*. 53.

[https://uknowledge.uky.edu/cbme\\_etds/53](https://uknowledge.uky.edu/cbme_etds/53)

This Master's Thesis is brought to you for free and open access by the Biomedical Engineering at UKnowledge. It has been accepted for inclusion in Theses and Dissertations--Biomedical Engineering by an authorized administrator of UKnowledge. For more information, please contact [UKnowledge@lsv.uky.edu](mailto:UKnowledge@lsv.uky.edu).

## **STUDENT AGREEMENT:**

I represent that my thesis or dissertation and abstract are my original work. Proper attribution has been given to all outside sources. I understand that I am solely responsible for obtaining any needed copyright permissions. I have obtained needed written permission statement(s) from the owner(s) of each third-party copyrighted matter to be included in my work, allowing electronic distribution (if such use is not permitted by the fair use doctrine) which will be submitted to UKnowledge as Additional File.

I hereby grant to The University of Kentucky and its agents the irrevocable, non-exclusive, and royalty-free license to archive and make accessible my work in whole or in part in all forms of media, now or hereafter known. I agree that the document mentioned above may be made available immediately for worldwide access unless an embargo applies.

I retain all other ownership rights to the copyright of my work. I also retain the right to use in future works (such as articles or books) all or part of my work. I understand that I am free to register the copyright to my work.

## **REVIEW, APPROVAL AND ACCEPTANCE**

The document mentioned above has been reviewed and accepted by the student's advisor, on behalf of the advisory committee, and by the Director of Graduate Studies (DGS), on behalf of the program; we verify that this is the final, approved version of the student's thesis including all changes required by the advisory committee. The undersigned agree to abide by the statements above.

Nicholas John Kohrs, Student

Dr. David A. Puleo, Major Professor

Dr. Abhijit R. Patwardhan, Director of Graduate Studies

SYNTHESIS AND CHARACTERIZATION  
OF BLUE LIGHT POLY( $\beta$ -AMINO ESTER)S

---

THESIS

---

A thesis submitted in partial fulfillment of the  
requirements for the degree of Master of Science  
in Biomedical Engineering  
in the College of Engineering  
at the University of Kentucky

By

Nicholas John Kohrs

Lexington, Kentucky

Director: David A. Puleo, Professor of Biomedical Engineering

Lexington, Kentucky

2018

Copyright © Nicholas John Kohrs 2018

## ABSTRACT OF THESIS

### SYNTHESIS AND CHARACTERIZATION OF BLUE LIGHT POLY( $\beta$ -AMINO ESTER)S

Volumetric muscle loss (VML) is a debilitating injury which results in full or partial loss of function. Current clinical options utilize tissue grafts and bracing to restore function. Tissue graft implantation oftentimes leads to serious complications, some of which end in graft rejection and thereby necessitate further surgeries and procedures. Polymeric scaffolds show promise as scaffolding systems due to their mechanical properties and overall degradation profiles. Scaffolds need appropriate mechanical properties, 10-60 kPa modulus, and overall degradation times, five days to two weeks, to initiate tissue regeneration. Poly( $\beta$ -amino ester)s (PBAE), a class of synthetic polymers, act as a safe biocompatible material with overall degradation times that are suitable for healing; however, due to harmful ultraviolet light (UV) irradiation from common crosslinking methods, these scaffold systems cannot be synthesized in vivo. This research presents the development and characterization of blue light (BL) crosslinked PBAEs. BL PBAEs showed vastly higher swelling ratios, 300-400% increase; decreased mechanical strength, an average decrease of 877 kPa in compressive modulus and 431 kPa in tensile modulus; and prolonged degradation patterns, 22% average mass retention. BL PBAEs show mechanical properties and degradation profiles that could be used as a skeletal muscle scaffolds.

Keywords: PBAE, volumetric muscle loss, scaffold, hydrogel, blue light

Nicholas John Kohrs

September 13, 2018

SYNTHESIS AND CHARACTERIZATION  
OF BLUE LIGHT POLY( $\beta$ -AMINO ESTER)S

By

Nicholas John Kohrs

David A. Puleo

Director of Thesis

Abhijit R. Patwardhan

Director of Graduate Studies

Date 10/25/18

## ACKNOWLEDGEMENTS

I would like to thank Dr. Puleo for giving me the opportunity to work in his lab. Dr. Puleo's knowledge and guidance was invaluable to this research. The wisdom and knowledge imparted to me will be invaluable for years to come. I would also like to thank Dr. Pham and Dr. Zhang for their help and expertise in this research.

I would also like to thank my family, especially my fiancée. Their support and encouragement during these last couple years has pushed me during this great endeavor. I would finally like to thank my labmates for their time and knowledge which helped advance my research.

## TABLE OF CONTENTS

ACKNOWLEDGEMENTS.....	iii
LIST OF TABLES .....	vi
LIST OF FIGURES.....	vii
INTRODUCTION.....	1
BACKGROUND AND SIGNIFICANCE.....	2
Wound healing response .....	2
Chronic wounds.....	5
Volumetric muscle loss.....	6
Clinical need.....	7
Regenerative approaches.....	7
Decellularized tissue scaffolds.....	8
Polymeric scaffolds .....	9
Poly( $\beta$ -amino ester) .....	10
Polymer crosslinking .....	10
Significance .....	11
MATERIALS AND METHODS.....	12
Materials.....	12
Macromer synthesis .....	12
Hydrogel fabrication.....	13
PBAE characterization.....	14
In Vitro degradation .....	14
Porosity.....	14
Mechanical testing .....	15

Drug release pilot study .....	15
Statistical analysis .....	16
RESULTS .....	17
Degradation study.....	17
PBAE degradation and swelling profiles .....	17
BL and UV degradation profiles.....	19
BL and UV swelling profiles .....	21
X-ray microtomography .....	23
pH profiles .....	26
Mechanical study.....	28
Compressive and tensile Modulus .....	28
Drug Release Pilot .....	32
DISCUSSION.....	33
CONCLUSION.....	39
APPENDIX .....	40
REFERENCES.....	44
VITA .....	49



## LIST OF TABLES

Table 1: FDA approved decellularized scaffolds.....	8
Table 2: Polymers for scaffold fabrication .....	9
Table 3: * BL and UV crosslinked hydrogel means which are statistically different are marked with asterisks (*) ( $p < 0.05$ ) .....	31

## LIST OF FIGURES

Figure 1: Summary of wound healing process .....	2
Figure 2: Normal wound healing process .....	4
Figure 3: Development of a chronic wound .....	6
Figure 4: (A) Chemical structures of diacrylates and amine used to form macromers. (B) Macromer synthesis reaction .....	12
Figure 5: Polymer degradation (a) and swelling (b) profiles for all UV hydrogels. Data are mean $\pm$ standard deviation (n = 9).....	18
Figure 6: BL and UV degradation profiles for hydrogels (a) AH6 3:1, (b) DH6 3:1, and (c) H6. Data are mean $\pm$ standard deviation (n = 9). Data sets AH6 3:1 and H6 exhibit UV and BL degradation curves which are statistically different (p < 0.05) after time point day 4 and hour 1.25, respectively .....	20
Figure 7: BL and UV swelling profiles for (a) AH6 3:1, (b) DH6 3:1, and (c) H6. Data are mean $\pm$ standard deviation (n = 9). All data sets are significantly different (p < 0.001) after time point day 1.26 (AH6 3:1), day 1.5 (DH6 3:1), and hour 0.66 (H6) .....	22
Figure 8: Porosity, pore size, and wall thickness between pores shown. Data are mean $\pm$ standard deviation (n = 3) .....	24
Figure 9: Evaluating hydrogel microarchitecture of BL and UV crosslinking methods. Data points which are significantly different are marked with a bar and asterisks (*) (p < 0.05). 25	25
Figure 10: pH of the hydrogel supernatant for A6 and D6. Data are mean $\pm$ standard deviation (n = 3).....	26
Figure 11: pH measurements for (a) AH6 3:1, (b) DH6 3:1, and (c) H6. Data are mean $\pm$ standard deviation (n = 3). Data points which are significantly different (p < 0.05) are marked with asterisks (*) .....	27
Figure 12: Representative load-deformation curves for (a) compression and (b) tensile testing of sample AH6 3:1 .....	28
Figure 13: Representative stress-strain curves for (a) compression and (b) tension. Red line indicates the slope of the given data used for calculating the modulus .....	29

Figure 14: Modulus for (a) compression and (b) tension. Data are mean  $\pm$  standard deviation (n = 4). Outliers are denoted by red plus signs .....30

Figure 15: Release of vancomycin and ketoprofen from DH6 3:1 BL and UV hydrogels, respectively (n = 1).....32

## INTRODUCTION

Volumetric muscle loss is a debilitating injury where the body is unable to heal, resulting in full or partial loss of function. The primary cause of volumetric muscle loss involves instances of high tissue loss such as traumatic injuries and surgical procedures. Commonly this injury results in the development of necrotic tissues, decreased strength and reduced range of motion. Depending upon the severity of the injury, treatment can vary from simple bracing techniques to complex surgical procedures; all with the ultimate aim of restoring function to the damaged tissues. The standard of care for this injury is the implantation of tissue grafts into the wound area.

Tissue implantation, autologous or allogenic, have several complications that affect the success of the implant. Immune response, disease transmission, donor site morbidity, and decreased range of motion and strength are all possible complications that could arise from treatment. All of these complications pose the risk of graft failure, resulting in another surgery to further remove necrotic tissue costing more time and money. Logistically, the lack of available tissue grafts further diminishes the viability of this treatment strategy.

This research focused on the development and characterization of a blue light (BL) poly ( $\beta$ -amino ester) (PBAE) system with the long term aim of in vivo polymerization. This system utilized a BL irradiation source with its water-soluble photoinitiator to allow PBAE crosslinking. Against the common UV crosslinking method, PBAEs were characterized by examining their physical and mechanical properties, more specifically: degradation and swelling profiles, changes in supernatant pH, modulus under tension and compression, and hydrogel microarchitecture. Characterizing the physical and mechanical properties of the BL PBAE scaffolding system allows for better insights to its possible applications.

## BACKGROUND AND SIGNIFICANCE

### Wound Healing Response

The wound healing response is a complex process involving many spatiotemporal overlapping processes including inflammation, tissue formation, and tissue remodeling [1-3]. Without any of these processes, healing cannot proceed and can lead to the development of chronic wounds. The wound healing process is shown in Figure 1. In normal wound healing immediately after occurrence of injury; vasoconstriction, of nearby vasculature, occurs as immune cells and platelets begin to flood to the wound area starting the clotting cascade.

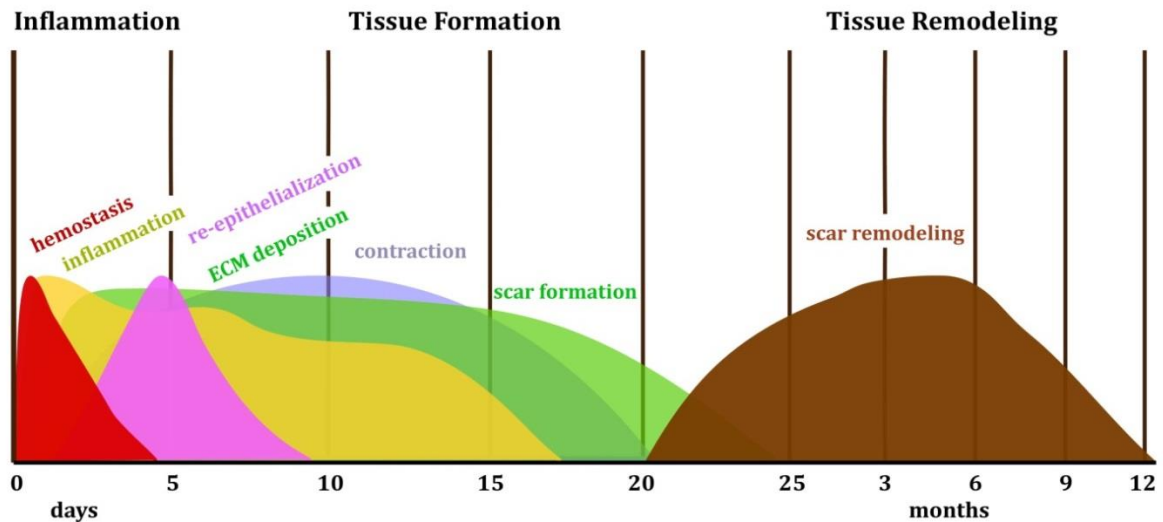


Figure 1: Summary of wound healing process. Adapted from Seifert, A.W., et al., *Skin Regeneration in Adult Axolotls: A Blueprint for Scar-Free Healing in Vertebrates*. PLoS ONE, 2012. 7(4): p. e32875.

As platelets invade the wound area they begin to come into contact with components of the extracellular matrix (ECM) causing release of numerous cytokines, chemokines, and growth factors; such as epidermal growth factor, transforming growth factor- $\beta$  (TGF- $\beta$ ), vascular endothelial cell growth factor (VEGF), and platelet-derived growth factor (PDGF)

[1, 4, 5]. This release causes further platelet aggregation and recruitment of fibrinogen to the wound area for the formation of a platelet plug; while simultaneously, the fibrinogen is converted into fibrin by thrombin. Fibrin is crosslinked and further stabilized by factor XIII to form a fibrin clot; which serves for local cell adhesion, modulates cell responses, and acts as a reservoir for growth factors, proteases, and protease inhibitors [6].

Near the end of the clotting cascade, the inflammation phase begins calling in multiple types of immune cells i.e. neutrophils, monocytes, and lymphocytes to the wound area, as seen in Figure 2 [4, 6]. Neutrophils are among the first immune cell to enter the wound area. Upon entering the wound area neutrophils begin to phagocytize any remnant tissue debris from the injury and form neutrophil extracellular traps to capture invading pathogens. These cells also have over 700 proteins stored inside including growth factors and pro-angiogenic factors, and upon activation can release these factors to aid in wound healing [7]. Apoptotic neutrophils aid in wound healing by releasing tissue repairing cytokines i.e. TGF- $\beta$  and Interleukin-10, further accelerating tissue repair [7]. Monocytes enter into the wound area and upon seeing the ECM become macrophages. These immune cells serve to remove spent neutrophils, apoptotic cells, and other debris; fight infection; promote and conclude inflammation; and secrete growth factors and cytokines e.g. TGF- $\beta$ , transforming growth factor  $\alpha$  (TGF- $\alpha$ ), heparin binding epidermal growth factor, fibroblast growth factor (FGF), and collagenase that activate and recruit endothelial cells, fibroblasts, and keratinocytes to the wound site [2, 4-6]. Little is known about the last immune cell to enter the wound area, lymphocytes; but there is evidence to suggest they play a role in the reorganization of keratinocytes and fibroblasts [4, 8]. The proliferative phase, in parallel with the inflammatory phase, is identified by angiogenesis and the formation of granulation

tissues [1, 4, 6]. The cytokines and growth factors, produced by the clotting cascade, begin to recruit fibroblasts, keratinocytes, and endothelial cells to the wound.

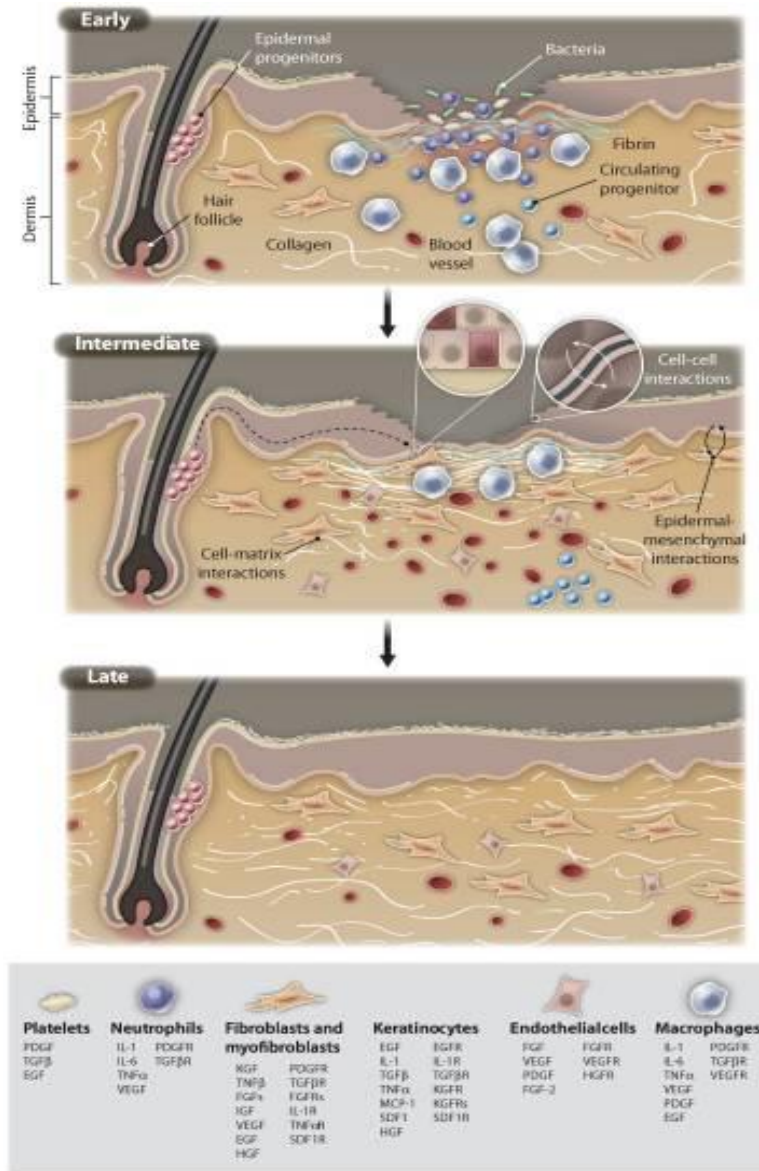


Figure 2: Normal wound healing process. From Eming, S.A., P. Martin, and M. Tomic-Canic, *Wound repair and regeneration: Mechanisms, signaling, and translation*. Science Translational Medicine, 2014. **6**(265): p. 265sr6-265sr6. Reprinted with permission from AAAS.

In response to growth factors such as PDGF, TGF- $\beta$ , and FGF; fibroblasts proliferate and produce new ECM materials e.g. collagen I & III, proteoglycans, and glycosaminoglycans [4]. Concurrently, capillary sprouts develop and begin to migrate into the wound, allowing for the transport of nutrients and oxygen to the surrounding tissues. Later in the proliferative stage, fibroblasts near the edge of the wound, differentiate into myofibroblasts, and overtime, close the wound. Remodeling of the microenvironment occurs over the next year as functionality is eventually restored to the damaged tissues. This is completed by altering ECM proteins from being mostly comprised of collagen III to collagen I via matrix metalloproteinases and the formation of collagen fiber bundles [9, 10].

### **Chronic Wounds**

Wound healing is a vastly complex process where the disturbance of any cellular or biochemical process could delay or prevent healing; bringing about chronic, non-healing wounds [5]. Non-healing wounds can develop at any time in the wound healing process i.e. inflammation, proliferation, and tissue remodeling. Healing oftentimes stalls during the inflammatory phase (Figure 3); as persistent inflammation causes an upregulation of pro-inflammatory cytokines, creating an excessive number of proteases leading to ECM degradation [11]. During proliferation, inappropriate levels of macrophages, fibroblasts, and keratinocytes can stall the wound healing process [4, 6, 8]. Tissue hypoxia, infection, disease, and age are other factors that inhibit wound healing. As stated, wound healing is a complex process involving many different signals, cells, and tissues in which the slightest miscue can cause the development of a chronic wound.



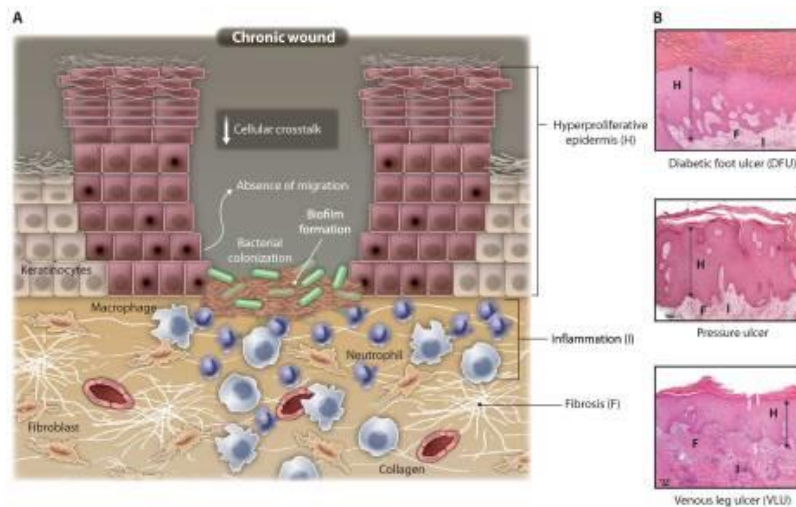


Figure 3. Development of a chronic wound. From Eming, S.A., P. Martin, and M. Tomic-Canic, *Wound repair and regeneration: Mechanisms, signaling, and translation*. Science Translational Medicine, 2014. **6**(265): p. 265sr6-265sr6. Reprinted with permission from AAAS.

### **Volumetric Muscle Loss**

For an average individual, skeletal muscle accounts for more than 40% of the total body mass [12]. Traumatic injuries, surgical procedures, and other incidences of high tissue loss are a few instances where the body is not able to heal and results in partial or total loss of function. These types of wounds are classified as volumetric muscle loss (VML). VML has been highly problematic for the military and its effects are seen in recent military conflicts i.e. Operation Enduring Freedom and Operation Iraqi Freedom; where the majority of injuries sustained involve severe musculoskeletal injury [13]. Of all battlefield injuries, 54% of cases present extremity injuries, with soft tissue injuries making up 53% of these cases. Due to these injuries countless military personnel have suffered partial or complete loss of function. VML cost the United States over 4 billion dollars in hospital expenses and loss of production (2010 data) [13]. VML not only affects military personnel but also civilians as an

estimated 4.5 million reconstructive surgeries involving tumor removals were completed in 2017 [14]. These procedures remove massive sections of tissue; oftentimes, leading to tissue deformation and loss of function. Not only does VML have an enormous economic cost but it also bears a huge psychological burden on the patient and the patient's family. The need for a viable treatment to VML has never been more pressing.

### **Clinical Need**

The standard of care is dependent upon the severity of the injury sustained, as bracing, tissue implantation, and regenerative strategies have been used to treat VML [3, 12, 13, 15-17]. Tissue implantation i.e. autologous implantation is the preferred method for dealing with severe cases of VML. In autologous implantation a tissue graft is taken from the patient and is used to replace damaged tissues, while minimizing the immune response from the body. One disadvantage of this system is the lack of available autologous grafts. Research is being conducted on allogenic muscle grafts as a possible option; however, the possibility of disease transmission and graft rejection are inherent disadvantages to using an allogenic transplant [18]. Even with the possibility of negating an immune response; donor site morbidity, loss of strength, and decreased function are common issues that diminish the viability of tissue implantation. Complications such as infection and tissue necrosis, cause 10% of these surgeries to fail [15]. While tissue implantation minimizes the immune response, better alternatives are needed to mitigate negative side effects and low implant availability.

### **Regenerative Approaches**

Regenerative medicine has been primarily focused on the development of scaffolding systems that mimic the ECM. These systems are designed to promote cell-biomaterial

interaction, control scaffold degradation and the exchange of important nutrients and growth factors, maintain mechanical stability with appropriately designed shape and microarchitecture, and elicit minimal response from the immune system [15, 19-22]. Current research focuses on the development of decellularized tissue scaffolds and the fabrication of polymeric scaffolds.

Decellularized Tissue Scaffolds

Currently several decellularized tissue scaffolds (Table 1) have been approved by the FDA. These scaffolds, mostly derived from bovine or porcine animals, are rich in latent growth factors such as basic fibroblast growth factor (bFGF) and vascular endothelial growth factor (VEGF), and have been shown to alter the wound microenvironment from one that induces fibrosis to one that promotes remodeling [23, 24].

Table 1: FDA approved decellularized scaffolds [18, 23]

<b>Products</b>	<b>Composition</b>
<b>OASIS Wound Matrix</b> ®	Acellular porcine small intestine submucosa
<b>PriMatrix</b> ®	Acellular fetal bovine dermis
<b>GraftJacket</b> ®	Acellular human dermis
<b>Integra</b> ®	Bilayer matrix bovine collagen and silicon
<b>MatriDerm</b> ®	Bovine collagen fibrils with elastin
<b>MySkin</b>	Cultured autologous keratinocytes on membrane
<b>EpiCel</b> ®	Cultured autologous keratinocytes
<b>Theraskin</b>	Human allogenic split-skin graft with keratinocytes and fibroblasts
<b>Regranex</b> ®	Human recombinant platelet-derived growth factor

Prior to implantation, decellularization i.e. removal of all cellular material, is needed to prevent immune responses. Poor decellularization is characterized by a massive inflammatory response which inhibits or prevents healing [24]. Decellularization is a harsh process and can affect the concentration of growth factors and proteins in these scaffolds

[15]. Along with limited availability, short shelf life, and inability to mass produce; alternative scaffold materials are needed.

Polymeric Scaffolds

Polymeric scaffolds are composed of biological or synthetic polymers. Biological and synthetic polymers are currently used to create scaffolds with specific mechanical, chemical, and biological properties that are tailored to a particular microenvironment. A variety of biological and synthetic polymers (Table 2) are being researched as scaffolding materials. Not only can these scaffolds be fabricated with specific characteristics but they can be loaded with growth factors, proteins, and drugs to aid in wound healing. The bioactivity of biological polymers has been shown to link certain growth factors i.e. VEGF and hepatocyte growth factor, to the scaffold, aiding in regeneration [19]. However, these scaffolds suffer from poor mechanical properties and oftentimes are used in conjunction with synthetic materials to ameliorate their poor mechanical properties.

Table 2: Polymers for scaffold fabrication

<i>Biological Polymers</i>	<i>Synthetic Polymers</i>
Collagen	Poly(glycolic acid) (PGA)
Chitosan	Poly-ε-caprolactone (PCL)
Alginate	Poly-l-lactic-acid (PLLA)
Agarose	Poly(lactic-co-glycolic-acid) (PLGA)
Fibrin	Poly(lactic acid) (PLA)
Gelatin	Poly(lactide-co-glycolide) (PLG)
Hyaluronic Acid	Polypeptides
Silk fibroin	Poly(acrylic acid) (PAA)
	Poly(ethylene oxide) (PEO)
	Poly (β-amino ester) (PBAE)

Synthetic polymers have the benefit of tailorable degradation profiles and architecture; however, these materials are plagued by the fact that they do not readily allow

cell attachment and are known to stimulate the foreign body response [15, 25]. This issue can be minimized by the addition of different proteins or macromolecules i.e. arginine–glycine–aspartic acid (RGD) peptides, to the scaffold’s microstructure [25, 26]. Due to variances in degradation and mechanical properties some polymers are suited for bone applications; whereas, others may be better suited for muscle or skin applications.

#### *Poly( $\beta$ -Amino Ester)*

Poly( $\beta$ -amino ester)s (PBAE), a class of synthetic polymers, were originally developed for gene and DNA delivery [27-30]. Current research is focused on using PBAEs as a scaffolding material. PBAEs are composed by step-growth conjugate addition reaction of diacrylate and amine groups [31, 32] and are known to be biodegradable via hydrolysis of the ester bonds and biocompatible [27, 33]. The byproducts from PBAE degradation are several small nontoxic molecules which can be readily cleared prior to reaching toxic levels [27, 34, 35]. Dependent upon the diacrylate and amine groups, tailorable degradation profiles, mechanical properties and shapes can be synthesized [27, 28, 33]. Designing PBAEs with certain physical, chemical, and mechanical properties allows for a multitude of applications.

#### **Polymer Crosslinking**

Different physical and chemical methods are being employed for polymeric crosslinking e.g. radical polymerization, high energy irradiation, enzymatic crosslinking, ionic interactions, and crystallization [36]. These different crosslinking methods allow for polymers to be fabricated with specific structure and properties. While these processes can crosslink polymers, they also produce unintended effects such as high cytotoxicity, low crosslinking, poor mechanical properties, etc. As such, choosing the method of crosslinking

is just as important as selection of the polymer. Photopolymerization is one of the primary methods used to crosslink polymeric materials. Despite toxic solvents and photoinitiators needed for crosslinking, UV irradiation is the primary crosslinking method for biomedical applications [37, 38]. To minimize the effect of harmful UV irradiation, current research has been working with different visible light irradiation sources i.e. green light, red light, and blue light (BL) [39-42]. One study is attempting to crosslink methacrylated hyaluronan with green light irradiation to act as an injectable tissue repair treatment system [41].

### **Significance**

The goal of this project was to develop and characterize a BL crosslinked PBAE, with the long term aim of in vivo crosslinking for VML applications. BL irradiation was chosen due to its slightly longer wavelength which has been shown to promote antimicrobial, antibacterial, and anti-inflammatory effects. [43-46]. In order for BL crosslinking to occur, a photoinitiator with an appropriate absorption spectra was selected. However, due to BL photoinitiator solubility issues, the BL crosslinking system was altered from the common UV crosslinking method to include BL irradiation and a water-soluble photoinitiator. With these changes, the BL system would be expected to minimize toxicity issues that the UV crosslinking method experienced.

The overall goal was to characterize BL PBAE scaffolds created by this method and compare it to the common UV crosslinking method. This was achieved by studying the systems physical and mechanical properties i.e. degradation and swelling profiles, changes in supernatant pH, Young's modulus under tension and compression, and hydrogel microarchitecture.

## METHODS AND MATERIALS

### Materials

Polyethylene glycol diacrylate (PEGDA 400) and diethylene glycol diacrylate (DEGDA) purchased from Polysciences, Inc. (Warrington, PA). Tetraethylene glycol diacrylate (TEGDA) purchased from TCI America (Portland, OR). Isobutylamine purchased from VWR international (Philadelphia, PA.). The photoinitiator (2,2'-Azobis[2-methyl-N-(2-hydroxyethyl)propionamide] (VA-086) was purchased from Wako Pure Chemical Industries, Ltd. (Richmond, VA). 2,2-Dimethoxy-2-phenylacetophenone (DMPA) and Ketoprofen was purchased from Sigma-Aldrich, Inc. (St. Louis, MO). Dichloromethane (DCM) and ethanol (EtOH) purchased from Pharmco-AAPER (Shelbyville, KY). Vancomycin was purchased from Gold Biotechnology (St. Louis, MO).

### Macromer Synthesis

Polyethylene glycol diacrylate (H), diethylene glycol diacrylate (A) and tetraethylene glycol diacrylate (D) were reacted with isobutylamine (6) using a 1.2:1 molar ratio of total acrylate to amine to form five different macromers [33, 47-49].

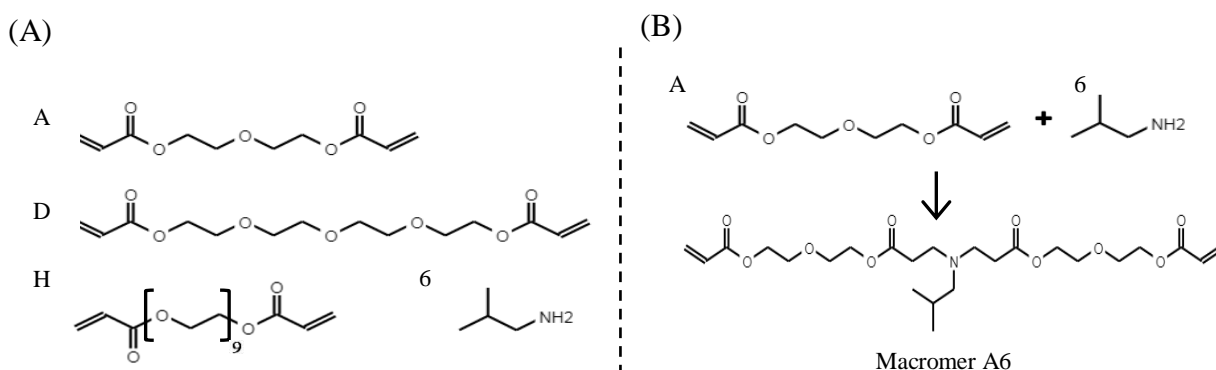


Figure 4: (A) Chemical structures of diacrylates and amine used to form macromers. (B) Macromer synthesis reaction.

Three single acrylate macromers were synthesized: H6, D6, and A6. While maintaining the molar ratio of total acrylate to amine, two macromers were synthesized with a 3:1 ratio of D to H (DH6 3:1) or A to H (AH6 3:1). These chemicals were pipetted into a round bottom flask with a magnetic stirrer. The flask was then placed in a silicon oil bath at 85°C and allowed to stir for 48 hours, at which point the reaction was quenched by cooling the macromer to 8° C. Macromer molecular weight was verified by gel permeation chromatography.

### **Hydrogel Fabrication**

Hydrogel samples were fabricated by free radical solution polymerization using either BL or UV to irradiate the solutions [33, 49]. For UV polymerization macromer solutions were synthesized by combining macromers with 1% (w/w) DMPA in 80% (w/w) DCM as compared to the macromer. For BL polymerization, macromer solutions followed similar preparation methods but the macromer was mixed with 2.8% (w/w) VA-086 in 80% (w/w) deionized water. To study the properties of both crosslinking systems, a variety of sample geometries were fabricated i.e., dogbones, discs, and cylinders. Due to differences in shape and solution volume, irradiation times varied from shape to shape. For dogbones and discs, the macromer solutions were pipetted between two glass slides separated by a 1.7 mm thick Teflon spacer and irradiated for 5 minutes with UV or 20 minutes by BL. Once crosslinked samples were then cut with either a 7.5 mm diameter punch or an ASTM D-1708 standard microtensile sample die. For cylinders, the macromer solution was pipetted into a glass cylinder mold, 5.8 mm diameter, and irradiated, with UV or BL, for 1 hour while being circumferentially exposed to the light on an in-house built instrument. Samples were then



washed overnight in an ethanol bath and allowed to dry. Once dried, cylinder samples were cut to a height to diameter ratio of 1.5:1.

## **PBAE Characterization**

### *In Vitro Degradation*

After measuring their initial mass, hydrogel discs were placed into 48-well plates, immersed in 1 ml of phosphate-buffered saline (PBS), pH 7.4, and gently shaken at 37 °C. At hydrogel dependent time points, hydrogel and PBS supernatant samples were collected. PBS supernatant samples were stored in 3 ml aliquots at -20 °C. For all samples the PBS supernatant was renewed in order to prevent the buildup of acidic supernatants. Once removed, hydrogel samples were dried of excess PBS and the wet mass was measured and compared to its initial mass to determine the swelling ratio. Samples were then stored at -20 °C for the duration of hydrogel degradation and then lyophilized for two days. Dry masses were then measured and compared to their initial masses to determine mass loss.

### *Porosity*

Hydrogel porosity was calculated by Scanco Medical X-ray microtomography (micro-CT). After dry mass measurements were taken, a triplicate of hydrogel samples from four specific degradation time points were taken and frozen at -20°C overnight and then lyophilized for two days. Samples were chosen to capture changes in hydrogel morphometry at critical points during degradation, i.e., the time points at the beginning, end, and before and after significant mass loss. Hydrogel microarchitectural differences were calculated by micro-CT analysis software. By measuring the area from each X-ray image, the micro-CT analysis software was able to calculate the porosity, pore size, and wall thickness between pores in the crosslinked hydrogels.

### Mechanical Testing

Evaluation of hydrogel modulus was accomplished by using a Bose Electroforce 3300 series test instrument with a 225 N force sensor measuring the load and deformation under confined compression and tensile testing. A strain rate of 0.05 mm/s and a preload of 0.1 N was selected for both compression and tensile testing. For compression and tensile sample geometries refer back to the hydrogel fabrication section, page 13. For compression testing, metal compression heads were mounted to the Bose system. Cylinder samples were then placed between two compression heads and compressed to 30% strain. For tensile testing, grips were attached to the movable heads of the Bose system. Silicone spacers were placed on both sides of the dogbone head, as to minimize failure and slippage near the grip section. Samples were placed in the grips and stretched to remove slack. The sample was then placed under tension until failure. For each sample run, the time (s), displacement (mm), and load (N) were collected in order to calculate the modulus. The modulus was calculated from the initial linear elastic region of the stress-strain curve.

### **Drug Release Pilot Study**

DH6 (BL) 3:1 and DH6 3:1 were studied for their respective release patterns. DH6 (BL) 3:1 was loaded with vancomycin while DH6 3:1 was loaded with ketoprofen. Both drugs were loaded at 10% (w/w) as compared to the macromer. After crosslinking, 7.5mm diameter samples were punched and placed into a 48-well plate and immersed in PBS. Every twelve hours supernatant was withdrawn, put into 6 ml tubes, and frozen. After a four day collection period, samples were thawed and measured by a BioTek PowerWave HT UV-Vis plate reader. Drugs were measured at different wavelengths: vancomycin (280 nm) and ketoprofen (310 nm).

## **Statistical Analysis**

A two-way analysis of variance (ANOVA) and Tukey's HSD post-hoc was run using R studio to statistically analyze the results for in vitro degradation and micro-CT studies. For mechanical testing, two-way ANOVA and multiple comparison post-hoc analysis was run using Matlab. Statistical significance was established at p values less than 0.05.

## RESULTS

### Degradation Study

#### PBAE Degradation & Swelling Profiles

PBAEs showed predictable degradation profiles, which exhibited minimal mass loss prior to a hydrogel-specific critical point, i.e. A6 day 30, D6 day 10, AH6 3:1 day 3.5, DH6 3:1 day 1.5, and H6 two hours, after which the samples began to rapidly lose mass, as seen in Figure 5 (a). Likewise, these critical points are near the maximum swelling of the hydrogels as seen in Figure 5 (b).

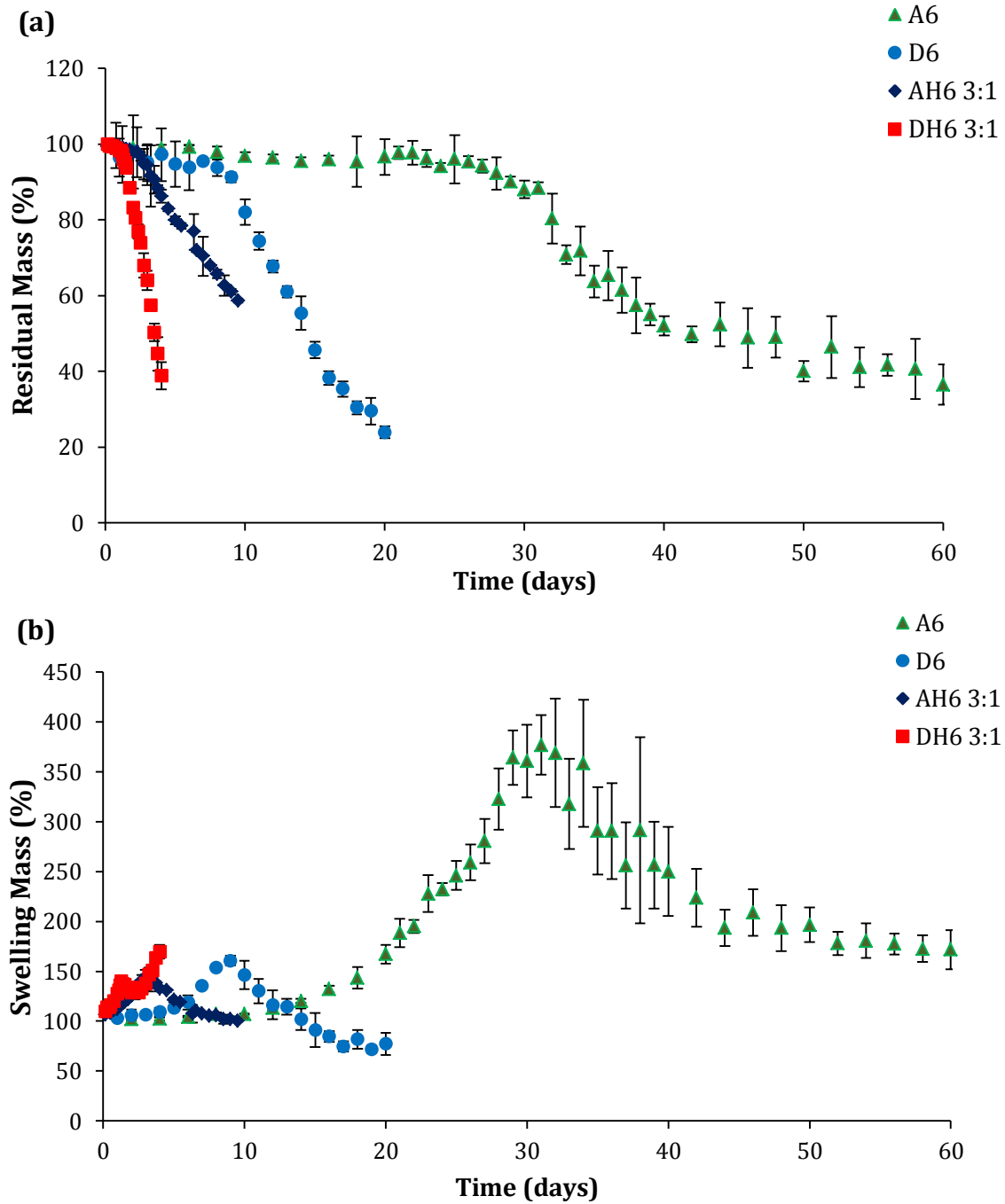


Figure 5: Polymer degradation (a) and swelling (b) profiles for all UV hydrogels. Data are mean  $\pm$  standard deviation ( $n = 9$ ).

### BL and UV Degradation Profiles

BL and UV hydrogels follow the typical degradation profile as seen in Figure 1.1, but BL hydrogels are shown to degrade differently compared to their UV counterparts: AH6 (BL) 3:1 degraded slower, H6 (BL) degraded quicker, and DH6 (BL) 3:1 degraded at the same speed (Figure 6). Two-way ANOVA showed statistically significant differences with respect to time point, crosslinking method, and the interaction between time point and crosslinking method ( $p < 0.05$ ).

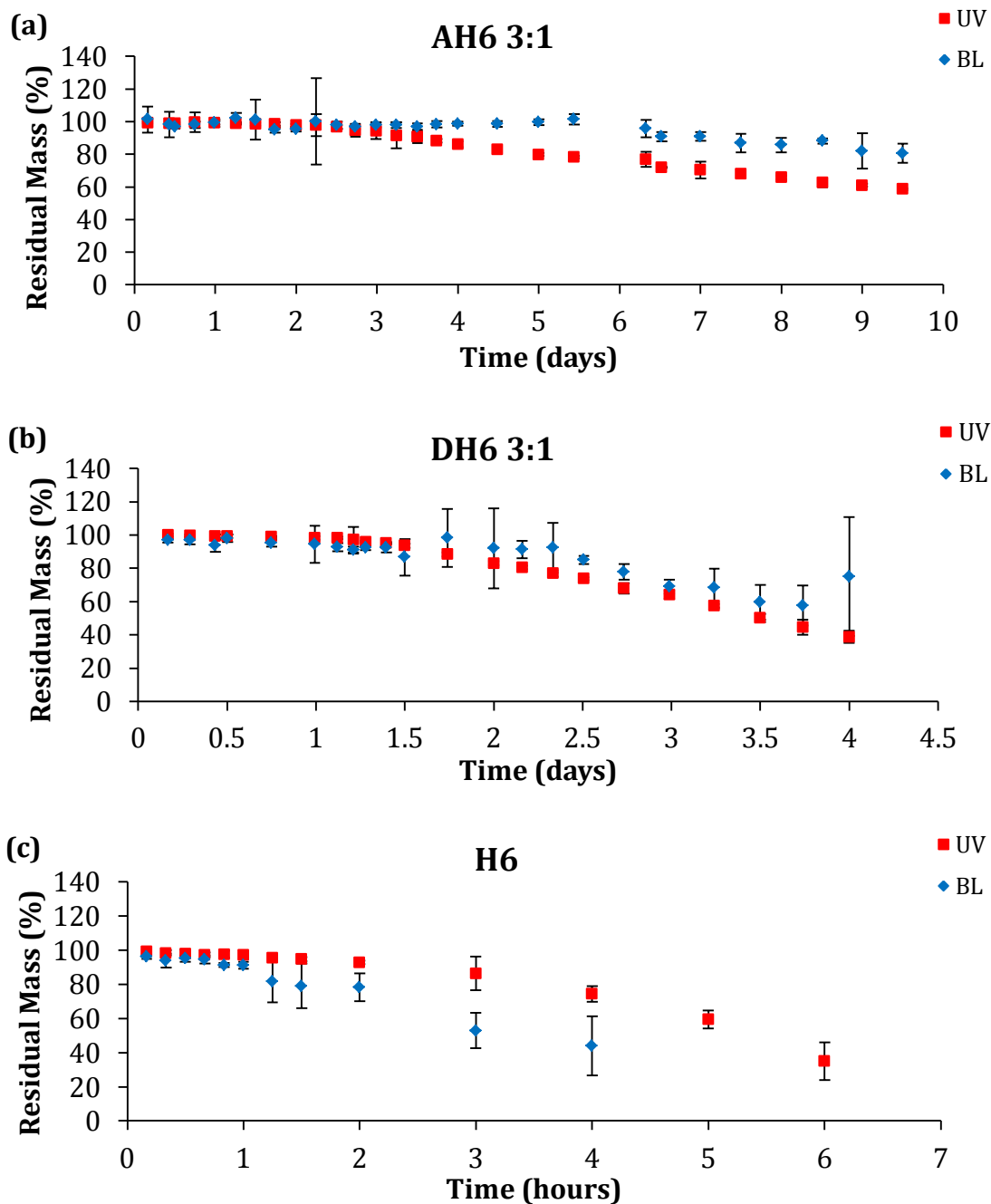


Figure 6: BL and UV degradation profiles for hydrogels (a) AH6 3:1, (b) DH6 3:1, and (c) H6. Data are mean  $\pm$  standard deviation ( $n = 9$ ). Data sets AH6 3:1 and H6 exhibit UV and BL degradation curves which are statistically different ( $p < 0.05$ ) after time point day 4 and hour 1.25, respectively.

### BL and UV Swelling Profiles

BL and UV PBAEs displayed significant differences when it came to swelling behavior, swelling from four to eight times their original mass (Figure 7). Two-way ANOVA shows that AH6 3:1, DH6 3:1, and H6 BL hydrogels were significantly different from their UV counterparts with respect to time point, crosslinking method, and the interaction between time point and crosslinking method ( $p < 0.05$ ).



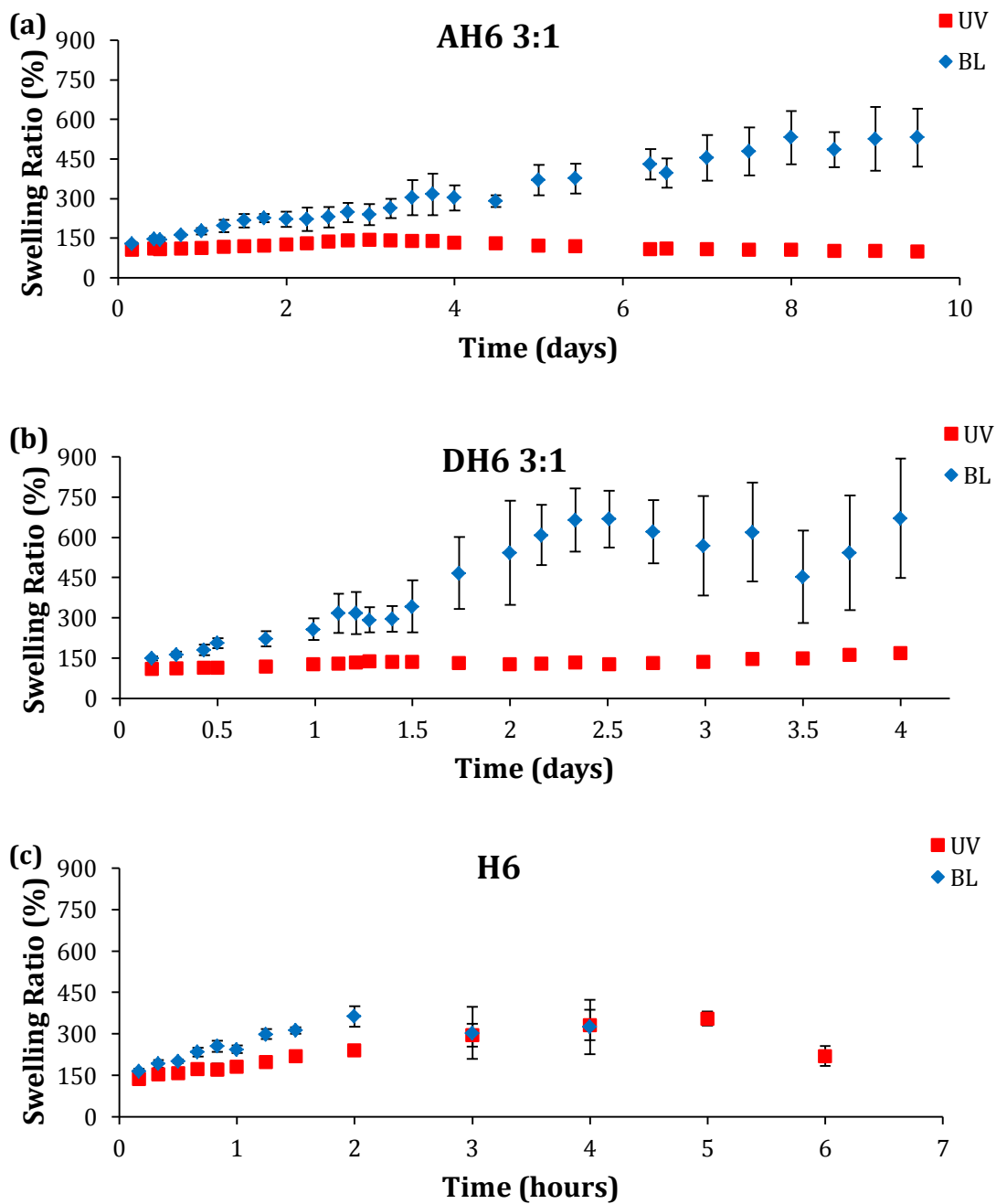


Figure 7: BL and UV swelling profiles for (a) AH6 3:1, (b) DH6 3:1, and (c) H6. Data are mean  $\pm$  standard deviation ( $n = 9$ ). All data sets are significantly different ( $p < 0.001$ ) after time point day 1.26 (AH6 3:1), day 1.5 (DH6 3:1), and hour 0.66 (H6).

### X-ray microtomography

MicroCT showed changing microarchitecture within the hydrogels during degradation. Throughout degradation BL hydrogels showed increasing porosity (Figures 8a), consistent pore sizes (Figure 8b), and decreasing wall thickness between pores (Figure 8c). Two-way ANOVA showed statistically significant differences between BL and UV hydrogels (Figure 9) showing statistical differences in porosity, pore size and wall thickness ( $p < 0.05$ )

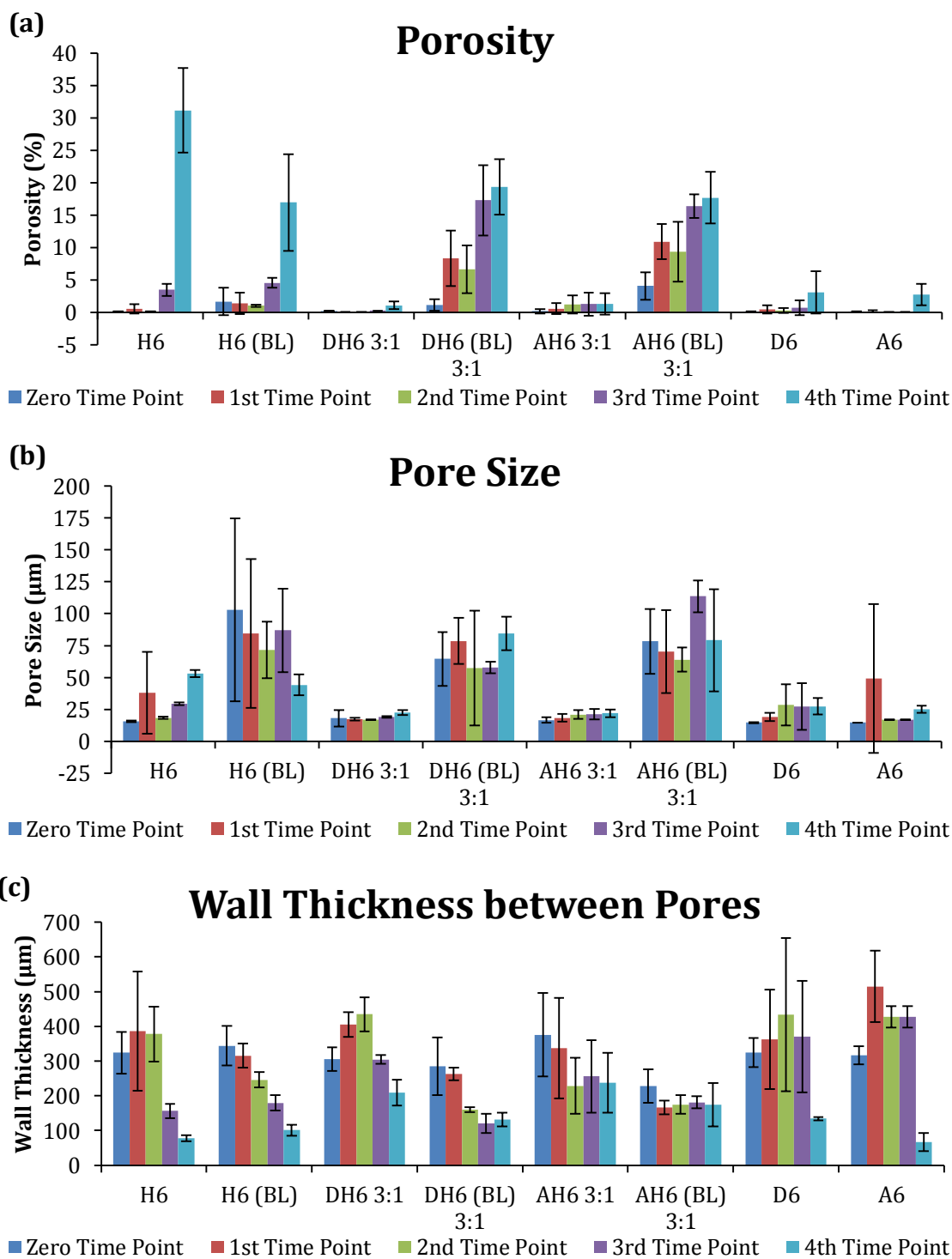


Figure 8: Hydrogel porosity, pore size, and wall thickness between pores shown. Data are mean  $\pm$  standard deviation ( $n = 3$ ).

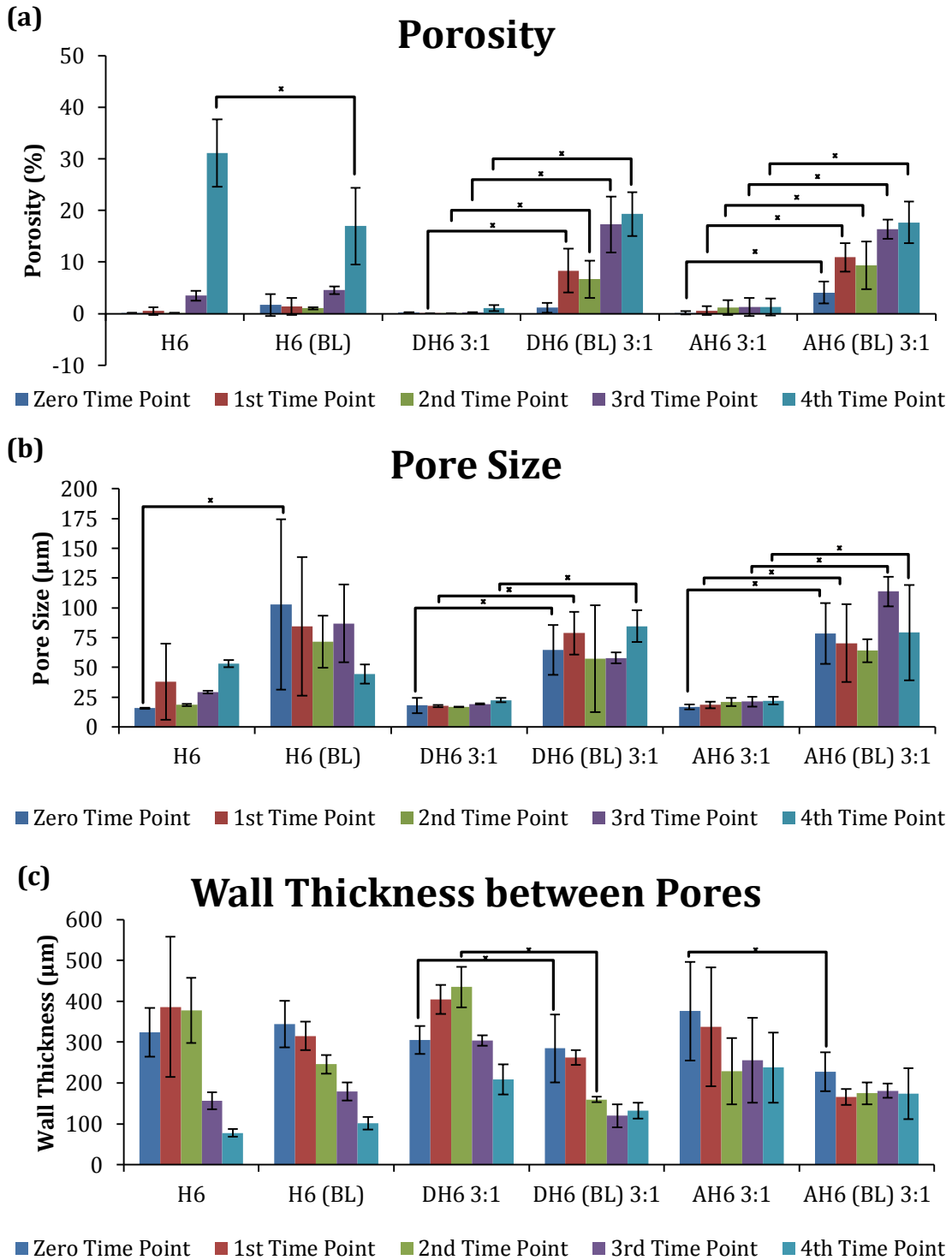


Figure 9: Evaluating hydrogel microarchitecture of BL and UV crosslinking methods. Data points which are significantly different are marked with a bar and asterisks (\*) ( $p < 0.05$ ).

### pH Profiles

The supernatant for hydrogels A6 and D6 started at a pH of 7.4, but near the critical point of mass loss, the pH dropped to a pH of 6.5 and then rose back to a pH of 7 (Figure 10). Instead of following this pattern, the other hydrogels, AH6 3:1, DH6 3:1, and H6, started with a pH slightly above 7.4 and showed a 0.5 pH unit drop over the span of degradation (Figure 11). Two-way ANOVA showed a statistically significant difference with respect to time point, crosslinking method, and the interaction between time point and crosslinking method ( $p < 0.05$ ).

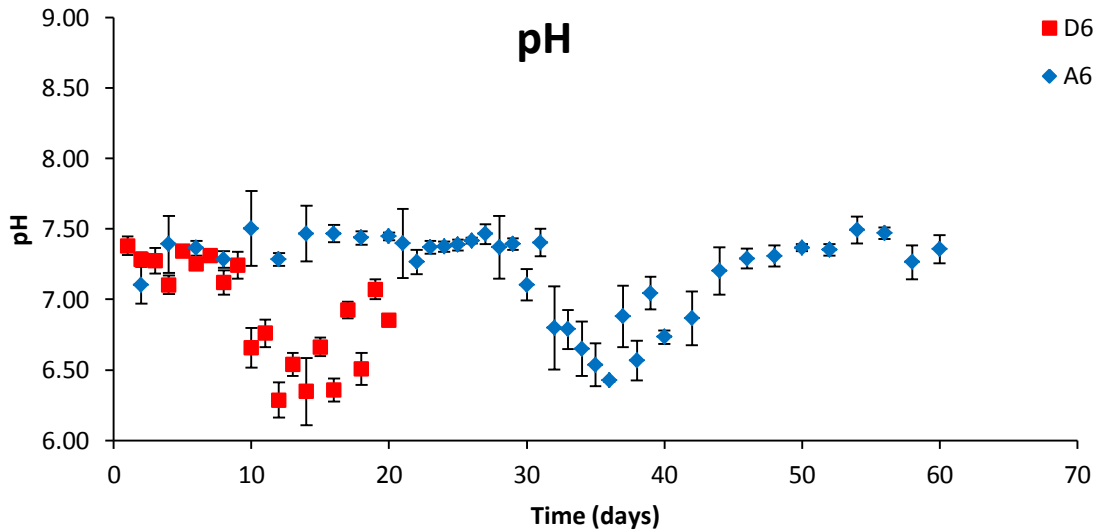


Figure 10: pH of the hydrogel supernatant for A6 and D6. Data are mean  $\pm$  standard deviation ( $n = 3$ ).

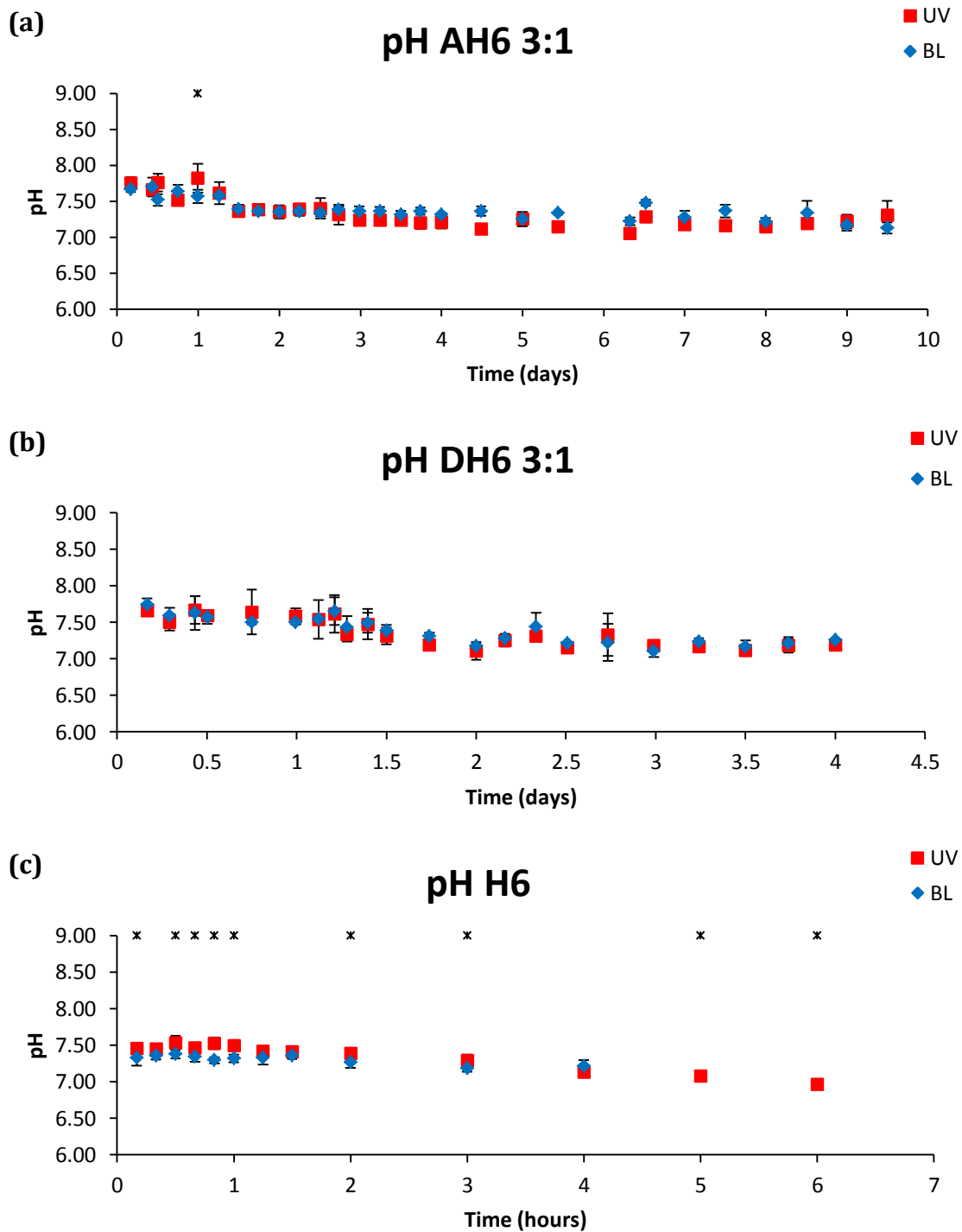


Figure 11: pH measurements for (a) AH6 3:1, (b) DH6 3:1, and (c) H6. Data are mean  $\pm$  standard deviation ( $n = 3$ ). Data points which are significantly different ( $p < 0.05$ ) are marked with asterisks (\*).

## Mechanical Study

### Compressive and Tensile Modulus

Load-deformation curves (Figure 12) were used to construct compressive (Figure 13a) and tensile (Figure 13b) stress-strain curves. These curves were then used to calculate the mean (Figure 14) and average (Table 3) modulus. BL hydrogels exhibited decreased compressive and tensile modulus as compared to UV crosslinked hydrogels. Two-way ANOVA showed statistically significant differences between crosslinking methods with BL and UV hydrogels AH6 3:1 and DH6 3:1 being statistically different ( $p < 0.05$ ).

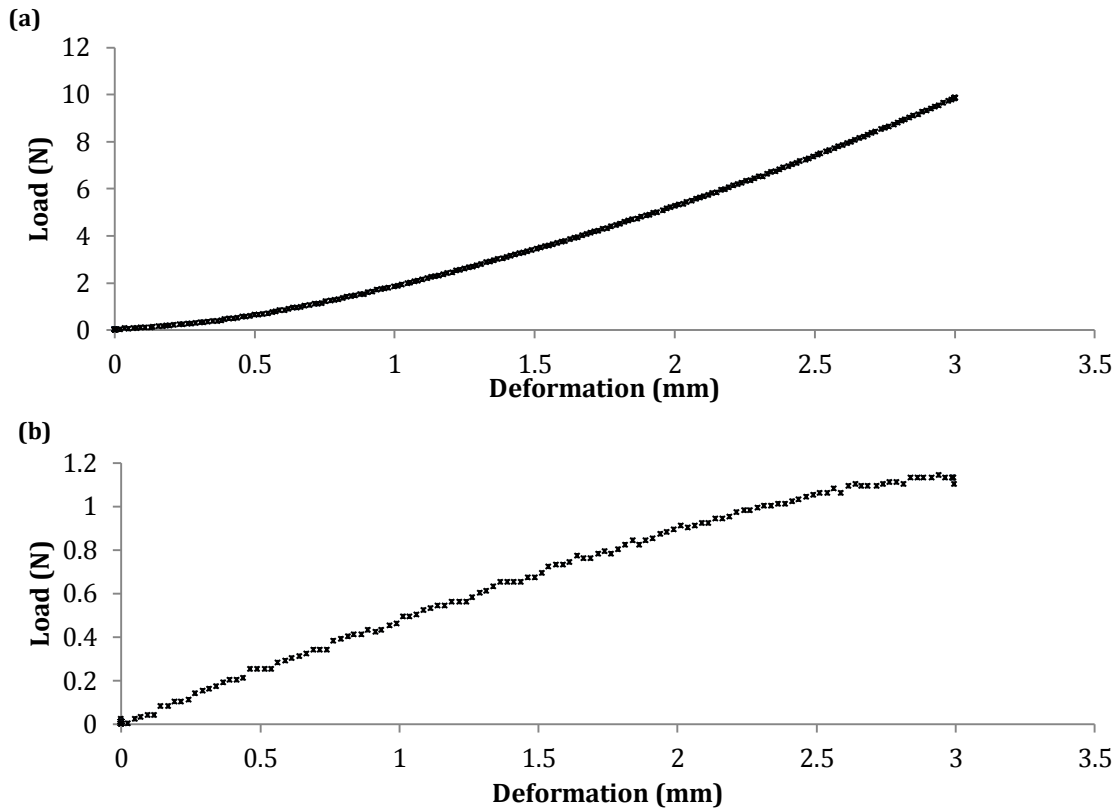


Figure 12: Representative load-deformation curves for (a) compression and (b) tensile testing of sample AH6 3:1

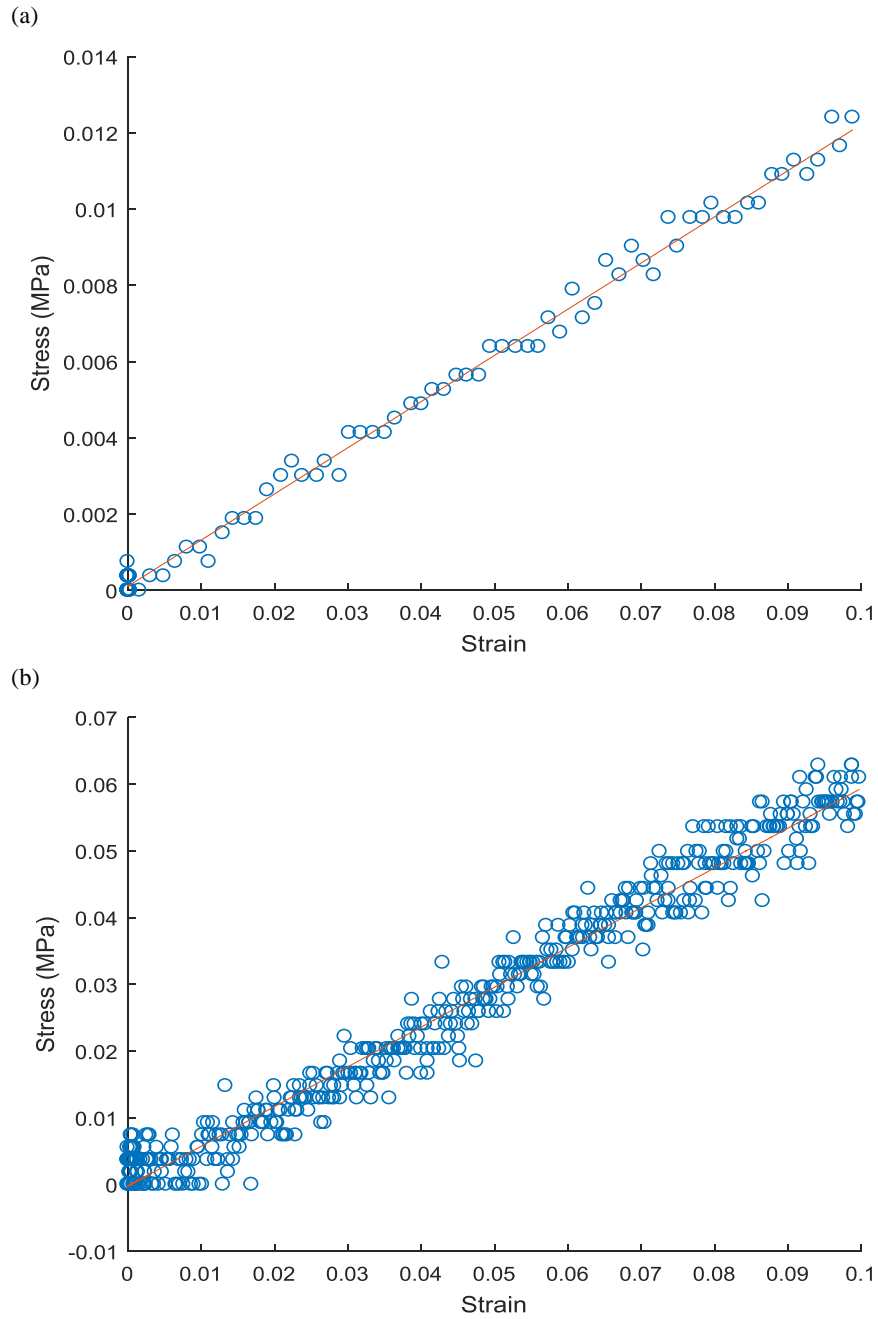


Figure 13: Representative stress-strain curves for (a) compression and (b) tension. Red line indicates the slope of the given data used for calculating the modulus.



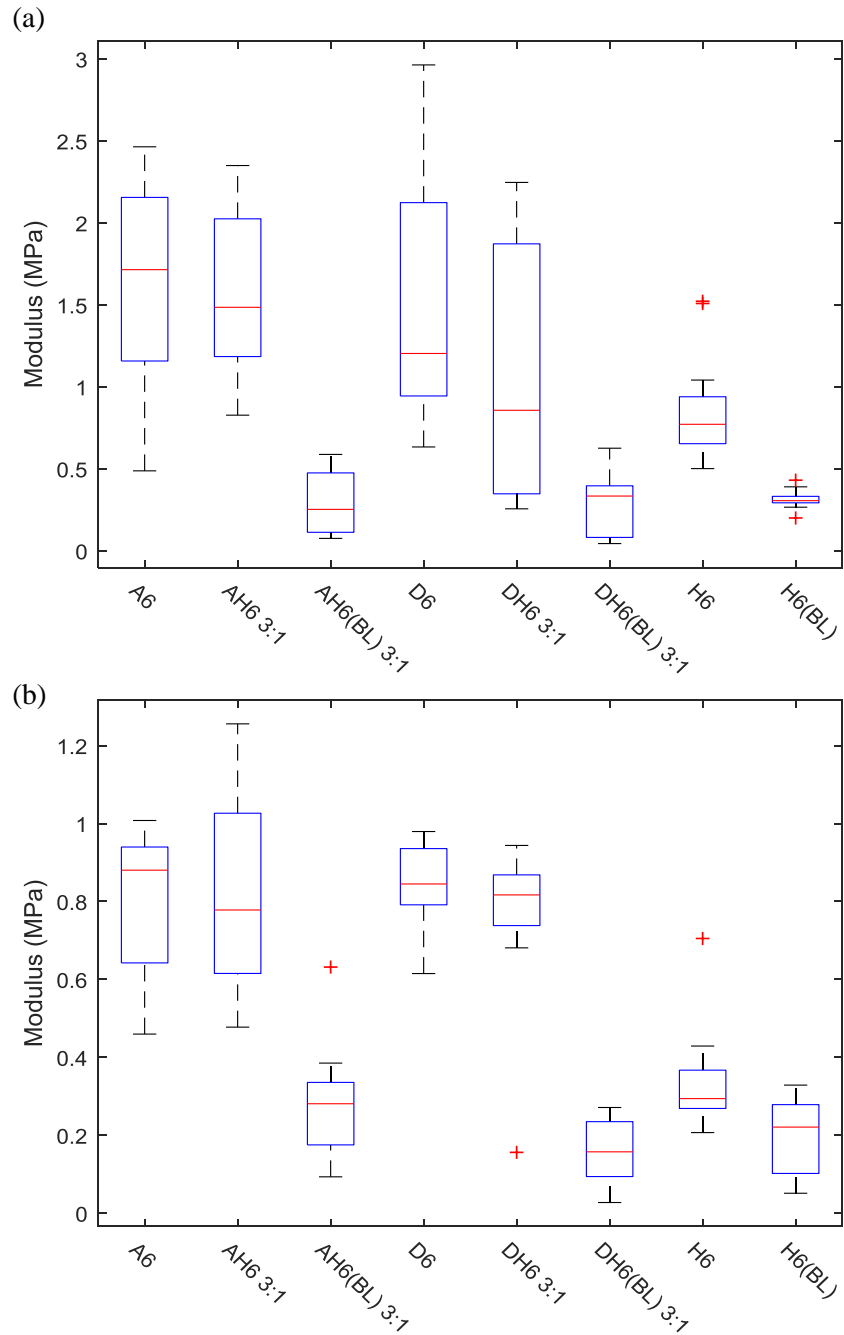


Figure 14: Modulus for (a) compression and (b) tension. Data are mean  $\pm$  standard deviation ( $n = 4$ ). Outliers are denoted by red plus signs.

Table 3: Average modulus of hydrogels.

Hydrogel	Average Compressive Modulus (KPa)	Average Tensile Modulus (KPa)
<b>A6</b>	1633 ± 607	801 ± 192
<b>D6</b>	1489 ± 725	835 ± 117
<b>AH6 3:1*</b>	1589 ± 499	821 ± 251
<b>AH6 (BL) 3:1*</b>	291 ± 204	279 ± 135
<b>DH6 3:1*</b>	1087 ± 798	776 ± 182
<b>DH6 (BL) 3:1*</b>	281 ± 194	160 ± 81
<b>H6</b>	840 ± 279	337 ± 129
<b>H6 (BL)</b>	313 ± 58	201 ± 96

\* BL and UV crosslinked hydrogel means which are statistically different are marked with asterisks (\*) ( $p < 0.05$ )

### Drug Release Pilot Study

Vancomycin and ketoprofen release from DH6 3:1 hydrogels. Vancomycin-loaded DH6 (BL) 3:1 hydrogels showed an initial burst release with a slow continual release until the end of the study. Ketoprofen-loaded DH6 3:1 hydrogels showed variable release patterns with a burst-like release in the middle of the study and an average release of almost four times that of vancomycin (Figure 15).

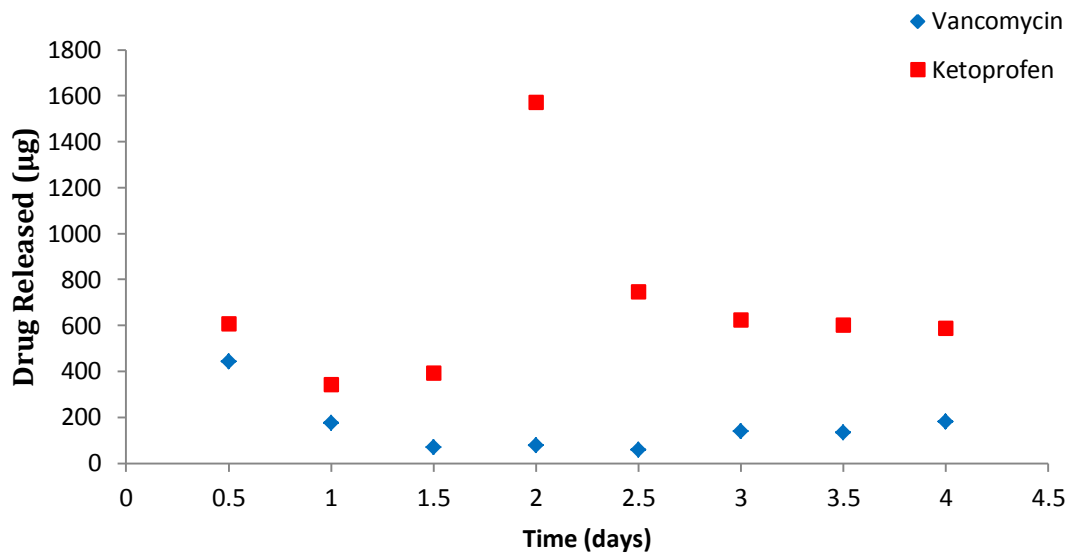


Figure 15: Release of vancomycin and ketoprofen from DH6 3:1 BL and UV hydrogels, respectively (n = 1).

## DISCUSSION

Poly( $\beta$ -amino ester)s, originally developed for gene and DNA delivery applications, have drawn significant interest as a scaffolding material. PBAEs have been previously reported as a safe biocompatible material [50, 51], with tailorable degradation profiles [33] and a wide range of mechanical properties [52]. In dealing with soft tissue injuries, appropriate degradation times and mechanical properties are necessary for tissue regeneration and cell penetration. Wound healing can take up to a year, depending upon the severity of the wound. Therefore, overall degradation needs to span a couple of weeks to allow the surrounding tissues enough time to replace the scaffold while not inhibiting tissue regeneration [15, 52-54]. In one study complete skeletal muscle formation occurred in 5 days [54]. BL PBAEs AH6 3:1 and DH6 3:1 lost 20% and 42% of their initial mass over 9.5 and 3.5 days, while their UV counterparts lost 41% and 50% of their initial mass over the same time, respectively. The degradation profiles for these PBAEs are shown to be appropriate for the formation of new skeletal muscle. Appropriate mechanical properties are also needed as they have been shown to influence cellular interactions i.e. cell adhesion and contractility [55], affect properties i.e. swelling [52], and play a key role in the wound healing process [56]. Skeletal muscle has been shown to have an average Young's modulus of  $\sim 10$  kPa [57-59] but has shown maximum values nearing 60 kPa [57, 59]. BL PBAEs AH6 3:1 and DH6 3:1 exhibited an average tensile modulus of  $279 \pm 135$  kPa and  $160 \pm 81$  kPa which is vastly decreased from the average tensile modulus of  $821 \pm 251$  kPa and  $776 \pm 182$  kPa posted by their UV counter parts.

PBAE degradation profiles and mechanical properties can be altered by changing either the diacrylate or amine in the macromer. In this research, varying the diacrylate elicited

different mechanical strengths and tailorable degradation profiles. Each diacrylate had a variance in the number of oxygens located in their monomer chain; see Figure 4 on page 12. This difference directly affected the hydrophobicity of the macromer, as having more oxygen in the monomer chain led to faster overall swelling and degradation.

Macromer molecular weight plays a role in PBAE degradation, swelling, and mechanical strength [27, 60]. Decreases in macromer molecular weight have been shown to cause increased crosslink density [28], therefore increasing the modulus and decreasing overall time of degradation. Variances in molecular weight allow for the formation of matrices with slightly different crosslink densities, which could cause minor variances in degradation, swelling, and mechanical properties. While macromer molecular weight could have an effect on degradation, swelling, and mechanical properties of PBAEs, it was not a focus of this research.

UV photopolymerization is the most common method of polymer crosslinking. This system boasts quick reaction times, with minimal heat production under physiological temperatures resulting in uniform hydrogel properties [61, 62]. This method is a double edged sword, as free radicals are needed for polymer crosslinking; yet, prolonged exposure to irradiation and free radicals [62] cause issues such as radiation safety and curing depth limitations [63]. Interest in visible light irradiation sources i.e. BL, have seen increased interest due to increased irradiation safety and energy utilization efficiency [63].

BL photopolymerization elicits different physical and mechanical properties as compared to the standard method. In this research BL crosslinking was impossible for two of these macromers: A6 and D6. These macromers were composed of diacrylates that had lower number of oxygens in their macromer chain which resulted in increased macromer

hydrophobicity. Attempting to mix the macromer with the aqueous photoinitiator solution resulted in a heterogeneous mixture which failed to crosslink. AH6 3:1 and DH6 3:1 faced similar issues but mixed completely, resulting in an opaque viscous solution which at times had difficulty crosslinking. H6 mixed completely and resulted in a transparent solution with an increased amount of gas bubbles.

The PBAEs formed from the BL crosslinking process displayed differences in degradation, swelling, and mechanical properties. The properties exhibited by these PBAEs, from their mechanical strength to degradation profile, are controlled by their specific structure. The combination of hydrophobicity, crosslink density, and microarchitecture induce hydrogel specific properties.

Hydrophobicity is one of the main factors affecting the structure and properties of these PBAEs. BL PBAEs are greatly impacted by macromer hydrophobicity, as hydrophobic macromers have increased difficulty in mixing homogeneously. This interaction created an opaque gaseous slurry, which could be the source of poor crosslinking and increased porosity and pore size. Degradation and swelling profiles are often dependent upon the hydrophobicity of their polymer, as the hydrophobic effect regulates the rate at which water interacts with the ester bonds. This interaction could explain why H6 BL degrades nearly two hours faster than its UV counterpart, as a good fraction of the bonds holding the matrix together may have already undergone hydrolysis during the fabrication process. The other BL hydrogels do not degrade as such, and are affected by other degradation factors affecting the structure of the hydrogel.

Crosslink density contributes to the different properties seen in BL PBAEs, specifically mechanical properties. BL PBAEs were difficult to handle as they would

oftentimes remaining tacky to the touch and tear easily. This suggests poor crosslinking has occurred, which has been correlated to decreased mechanical strength, increased swelling, and faster overall degradation [64-68]. BL hydrogels follow this trend seeing decreased mechanical strength and a massive increase in swelling; however, BL hydrogels AH6 3:1 and DH6 3:1 deviate from this pattern seeing degradation profiles which initially mimicked UV hydrogels but near the end of degradation began to see statistically different measurements. In this case poor crosslinking does not act as the main affecter, as poor crosslinking should cause a decrease in overall time of degradation, not an increase. A possible explanation for the slower overall degradation profile is the formation of hydrophobic aggregates. The degree to which the macromer and water mixed is unknown and could have resulted in the formation of a heterogeneous matrix with hydrophobic aggregates. These areas would inhibit water infiltration and thus slow degradation.

As seen in the results section, BL hydrogels have higher initial porosities and pore sizes, seeing increases in both throughout degradation; whereas, UV hydrogels maintained minimal porosity and constant pore sizes. H6 did not follow this trend, as both UV and BL samples had similar porosities and pore sizes throughout degradation. Hydrogel microarchitecture has been shown to influence mechanical strength and swelling capacity, as increased porosity and pore size indicate increased swelling ratios [67, 69] and decreased mechanical strengths [65, 66, 69].

During the degradation process there is a point prior to hydrogel mass loss that sees alterations in degradation, swelling, and pH profiles. Beyond this critical point, the hydrogel loses mass at a significant rate, sometimes losing as much as 30% of the original mass within a few measurements. At this point during degradation, there is a noticeable drop in pH for

two of the more hydrophobic hydrogels: A6 and D6. All other hydrogels see only a slight drop in the pH over the period of degradation. During the process of hydrolysis, ester bonds are broken down into carboxylic acid and an alcohol. One possibility for the difference in pH between hydrogels is different rates of PBAE degradation. Different PBAE degradation rates would cause different rates of acid production possibly explaining the buildup of acid in PBAEs A6 and D6. While there are periods of increasing acidity, the body is able to regulate the pH of the interstitial fluid thus clearing any acidic build up from the body. A stable pH level is critical for the scaffolds integrity and biocompatibility, as too much acidic stress could induce an inflammatory response preventing proper integration and eventually leading to massive fibrosis.

BL PBAEs demonstrate the ability to release drug from their matrix in a controllable manor. Controlled release of drugs or growth factors to attain therapeutic levels is a high priority in the field of tissue engineering. With controllable degradation and swelling profiles, PBAEs exhibit their ability to release growth factors and other therapeutic drugs for tissue regeneration applications [70, 71]. Current PBAE systems utilize an organic solvent system which lacks the ability to homogenously distribute water-soluble drugs throughout the scaffold. BL PBAEs are able to achieve uniform water-soluble drug distribution. Vancomycin and ketoprofen were used to look at the release patterns of drugs from the BL and UV crosslinked PBAEs. These drugs were selected for their solubility in each solvent system. PBAEs released their respective drugs at slightly different levels at different times. UV samples seemed to release a majority of their drugs near the end of the study while BL hydrogels tended to release their drug at the beginning of the study. Vancomycin is relatively larger than ketoprofen; however, the difference in size does not seem to play a major role in



the release of these drugs. If size played a role then ketoprofen, being the smaller molecular weight drug, would release most of the drug at the beginning of the study. One explanation is differences in hydrogel structure. BL hydrogels have been shown to be poorly crosslinked leading to the possibility of early release from the matrix; whereas, UV hydrogels have an increased crosslink density allowing for the drug to stay longer inside of the matrix. BL hydrogels released a lower amount of total drug suggesting poor loading. One explanation for the lower drug release is the EtOH washing phase. As the hydrogel undergoes washing to remove any unreacted monomers and photoinitiator solutions, the drug may have been washed away as well only leaving the strongly entrenched drug molecules behind. As a proof of concept, drugs can be loaded and released from the BL hydrogels.

## CONCLUSION

Understanding how changes in hydrogel structure and properties affect their function gives great insight to their possible applications. The aim of this project was to develop a hydrogel system with the future aim being a regenerative strategy for wound healing applications. This research developed BL PBAE hydrogels and evaluated the differences between UV and BL hydrogels. BL PBAEs exhibit increased swelling ratios, prolonged degradation, and a decreased modulus. The properties of these PBAEs have mechanical strengths and degradation profiles that are appropriate for use in skeletal muscle scaffolding systems. BL PBAEs could be used in drug delivery applications for the delivery of water-soluble drugs due to their degradation and swelling profiles. Further study is needed to attain appropriate mechanical properties and evaluate the possible drug release applications of BL PBAEs.

## APPENDIX

### CELL STUDIES

#### Materials

Trypan blue and Dulbecco's modified Eagle's medium (DMEM) purchased from HyClone (Logan, UT). Thiazolyl blue tetrazolium bromide (MTT reagent), Bovine Serum Albumin (BSA), and Hoechst 33258 purchased from Thermo Fisher Scientific Chemicals Inc. (Ward Hill, MA)., Fibronectin, collagen I, collagen III, and tenascin C purchased from Millipore Sigma (Burlington, MA).

#### Methods

To understand how different ECM backgrounds alter cellular proliferation and attachment; a comparison between the regenerative *Acomys* (SM1) and the non-regenerative *Mus musculus* (M2) was completed. Immortalized fibroblast cell lines from these animals were seeded on different coating backgrounds and assayed. Six different coating backgrounds were selected for this study: fibronectin, collagen I, collagen III, tenascin C, bovine serum albumin (BSA), and tissue culture plastic (TCP).

Table 4: Protein Concentration

Protein	Concentration ( $\mu\text{g/ml}$ )
Tenascin C	1.52
Fibronectin	1.73
Collagen I	1.73
Collagen III	1.17
Albumin	0.92

These ECM protein backgrounds were coated on 24-well TCP plates at concentrations to obtain a surface density that would form a protein monolayer (Table 3) [72,

73]. Each well was coated by adding 100  $\mu$ L of an individual protein concentration and were given two hours at room temperature for protein adsorption. The plates were then washed twice with PBS and a 5% BSA in PBS blocking solution was applied for 2 hours at room temperature. Wells were washed with PBS two more times and air dried and stored at 2-8  $^{\circ}$ C for future use. Both cell lines were detached and seeded using basic cell culture methods. The attachment assay was seeded at 40,000 cells per well, while the proliferation assay was seeded at 1,000 cells per well.

Both assays were allowed to run for specified times as to observe the attachment and proliferation of the individual cell lines. The attachment assay had four time points at 0.5, 1, 2, and 4 hours, while the proliferation assay was measured once daily for six days. The assays were measured using the Hoechst DNA quantification protocol [74]. At the time of lysis, cells are washed twice with PBS, and 1 ml of a lysis buffer (0.05 M  $\text{NaH}_2\text{PO}_4$ , 2 M NaCl, 2 mM EDTA, pH 7.4) was added. Each well was sonicated two times for 10 seconds, and 0.25 ml of 2  $\mu$ g/ml Hoechst 33258 was added to each well, shaken gently, and left at room temperature in the dark for 10 minutes. Fluorescence was measured at  $\lambda_{\text{ex}} = 356$  nm and  $\lambda_{\text{em}} = 458$  nm.

### **Preliminary Results**

Initial results showed differences in attachment and proliferation, both qualitatively and quantitatively. Mus fibroblasts showed to attach quicker and at higher numbers, while Acomys fibroblasts showed increased proliferation. Prior to starting the study was unable to keep healthy low passage cell lines. Study was halted as to focus on material study. Two-way ANOVA showed statistical differences in proliferation between Acomys and Mus fibroblasts ( $p = 0.05$ ); however, attachment was not statistically different.

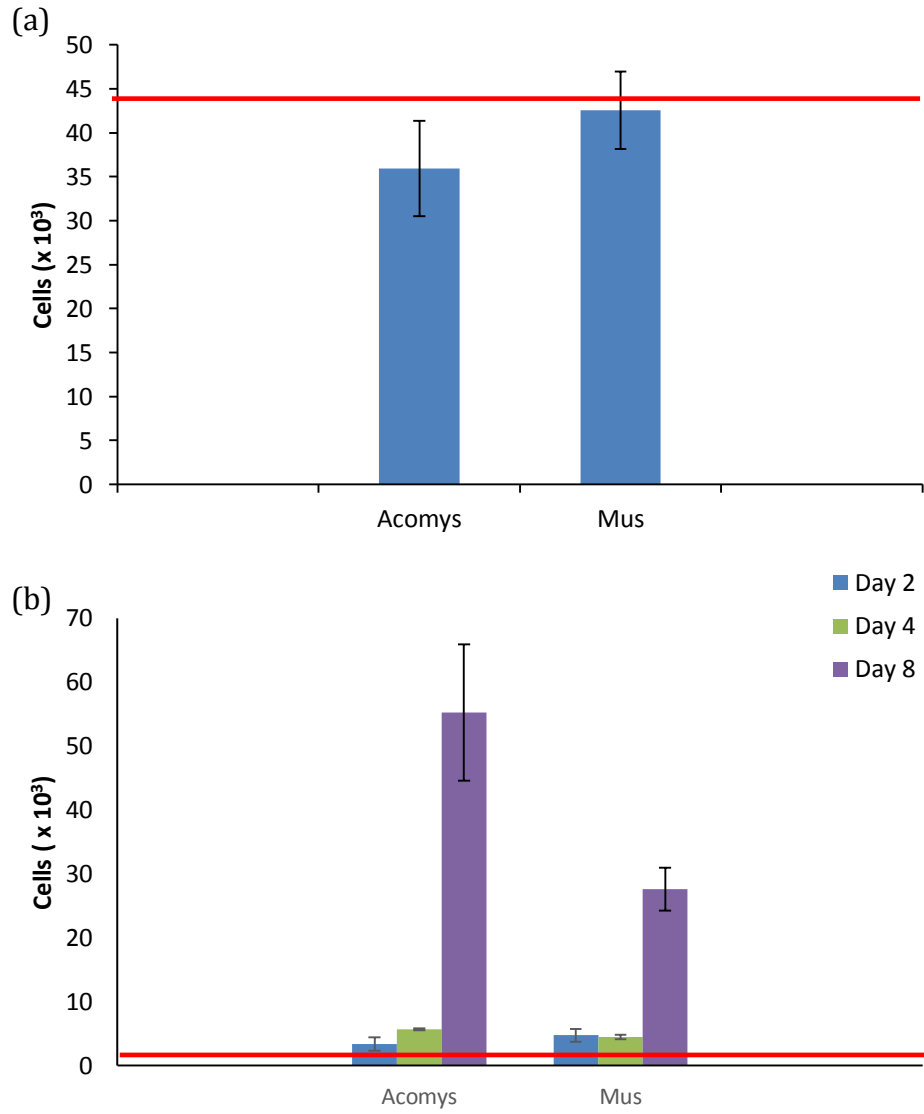


Figure 16: Mus and Acomys fibroblast (a) attachment and (b) proliferation studies. Cells were seeded at 40K and 1K for attachment and proliferation studies. Red line indicates cell seeding. Data are mean  $\pm$  standard deviation (n=3).

## **Discussion**

There is a prevalent need to understand how cellular attachment and proliferation are affected by different protein backgrounds. Understanding cellular responses to different protein backgrounds will allow future work to focus on the best protein combination to aid in a wound healing environment.

## REFERENCES

1. Eming, S.A., P. Martin, and M. Tomic-Canic, *Wound repair and regeneration: Mechanisms, signaling, and translation*. Science translational medicine, 2014. **6**(265): p. 265sr6-265sr6.
2. Seifert, A.W., et al., *Skin Regeneration in Adult Axolotls: A Blueprint for Scar-Free Healing in Vertebrates*. PLoS ONE, 2012. **7**(4): p. e32875.
3. Takeo, M., W. Lee, and M. Ito, *Wound Healing and Skin Regeneration*. Cold Spring Harbor Perspectives in Medicine, 2015. **5**(1): p. a023267.
4. Sgonc, R. and J. Gruber, *Age-Related Aspects of Cutaneous Wound Healing: A Mini-Review*. Gerontology, 2013. **59**(2): p. 159-164.
5. Velnar, T., T. Bailey, and V. Smrkolj, *The wound healing process: an overview of the cellular and molecular mechanisms*. J Int Med Res, 2009. **37**(5): p. 1528-42.
6. Schultz, G.S., et al., *Dynamic Reciprocity in the Wound Microenvironment*. Wound repair and regeneration : official publication of the Wound Healing Society [and] the European Tissue Repair Society, 2011. **19**(2): p. 134-148.
7. Wang, J., *Neutrophils in tissue injury and repair*. Cell and Tissue Research, 2018. **371**(3): p. 531-539.
8. Martin, P. and R. Nunan, *Cellular and molecular mechanisms of repair in acute and chronic wound healing*. The British Journal of Dermatology, 2015. **173**(2): p. 370-378.
9. Gurtner, G.C., et al., *Wound repair and regeneration*. Nature, 2008. **453**: p. 314.
10. Shaw, T.J. and P. Martin, *Wound repair at a glance*. Journal of Cell Science, 2009. **122**(18): p. 3209-3213.
11. Frykberg, R.G. and J. Banks, *Challenges in the Treatment of Chronic Wounds*. Advances in Wound Care, 2015. **4**(9): p. 560-582.
12. Aguilar, C.A., et al., *Multiscale analysis of a regenerative therapy for treatment of volumetric muscle loss injury*. Cell Death Discov, 2018. **4**: p. 33.
13. Corona, B.T., et al., *Volumetric muscle loss leads to permanent disability following extremity trauma*. J Rehabil Res Dev, 2015. **52**(7): p. 785-92.
14. *2017 Plastic Surgery Statistics Report*. American Society of Plastic Surgeons, 2017.
15. Grasman, J.M., et al., *Biomimetic Scaffolds for Regeneration of Volumetric Muscle Loss in Skeletal Muscle Injuries*. Acta biomaterialia, 2015. **25**: p. 2-15.
16. Grogan, B.F. and J.R. Hsu, *Volumetric muscle loss*. J Am Acad Orthop Surg, 2011. **19 Suppl 1**: p. S35-7.
17. Sicari, B.M., et al., *An acellular biologic scaffold promotes skeletal muscle formation in mice and humans with volumetric muscle loss*. Sci Transl Med, 2014. **6**(234): p. 234ra58.
18. Ho, J., et al., *Current Advancements and Strategies in Tissue Engineering for Wound Healing: A Comprehensive Review*. Advances in Wound Care, 2017. **6**(6): p. 191-209.
19. Fuoco, C., et al., *Matrix scaffolding for stem cell guidance toward skeletal muscle tissue engineering*. Journal of Orthopaedic Surgery and Research, 2016. **11**: p. 86.
20. O'Brien, F.J., *Biomaterials & scaffolds for tissue engineering*. Materials Today, 2011. **14**(3): p. 88-95.

21. Rodríguez-Vázquez, M., et al., *Chitosan and Its Potential Use as a Scaffold for Tissue Engineering in Regenerative Medicine*. BioMed Research International, 2015. **2015**: p. 821279.
22. Williams, D.F., *The Biomaterials Conundrum in Tissue Engineering*. Tissue Engineering Part A, 2014. **20**(7-8): p. 1129-1131.
23. Turner, N.J. and S.F. Badylak, *Biologic scaffolds for musculotendinous tissue repair*. Eur Cell Mater, 2013. **25**: p. 130-43.
24. Keane, T.J., I.T. Swinehart, and S.F. Badylak, *Methods of tissue decellularization used for preparation of biologic scaffolds and in vivo relevance*. Methods, 2015. **84**: p. 25-34.
25. Swartzlander, M.D., et al., *Immunomodulation by Mesenchymal Stem Cells Combats the Foreign Body Response to Cell-Laden Synthetic Hydrogels*. Biomaterials, 2015. **41**: p. 79-88.
26. Drury, J.L. and D.J. Mooney, *Hydrogels for tissue engineering: scaffold design variables and applications*. Biomaterials, 2003. **24**(24): p. 4337-4351.
27. Hawkins, A.M., et al., *Synthesis and analysis of degradation, mechanical and toxicity properties of poly( $\beta$ -amino ester) degradable hydrogels*. Acta biomaterialia, 2011. **7**(5): p. 1956-1964.
28. M., H.A., P.D. A., and H.J. Zach, *Effect of macromer synthesis time on the properties of the resulting poly( $\beta$ -amino ester) degradable hydrogel*. Journal of Applied Polymer Science, 2011. **122**(2): p. 1420-1426.
29. Perni, S. and P. Prokopovich, *Poly-beta-amino-esters nano-vehicles based drug delivery system for cartilage*. Nanomedicine: Nanotechnology, Biology and Medicine, 2017. **13**(2): p. 539-548.
30. Green, J.J., et al., *Poly ( $\beta$ -amino esters): Procedures for Synthesis and Gene Delivery*. Methods in molecular biology (Clifton, N.J.), 2009. **480**: p. 53-63.
31. Meenach, S.A., et al., *Controlled synergistic delivery of paclitaxel and heat from poly(beta-amino ester)/iron oxide-based hydrogel nanocomposites*. Int J Pharm, 2012. **427**(2): p. 177-84.
32. Metter, R.B., et al., *Biodegradable fibrous scaffolds with diverse properties by electrospinning candidates from a combinatorial macromer library*. Acta Biomaterialia, 2010. **6**(4): p. 1219-1226.
33. Hawkins, A.M., et al., *Tuning biodegradable hydrogel properties via synthesis procedure*. Polymer, 2013. **54**(17): p. 4422-4426.
34. Green, J.J., R. Langer, and D.G. Anderson, *A combinatorial polymer library approach yields insight into nonviral gene delivery*. Acc Chem Res, 2008. **41**(6): p. 749-59.
35. Lynn, D.M. and R. Langer, *Degradable Poly( $\beta$ -amino esters): Synthesis, Characterization, and Self-Assembly with Plasmid DNA*. Journal of the American Chemical Society, 2000. **122**(44): p. 10761-10768.
36. Hennink, W.E. and C.F. van Nostrum, *Novel crosslinking methods to design hydrogels*. Advanced Drug Delivery Reviews, 2002. **54**(1): p. 13-36.
37. Greene, T., et al., *Comparative study of visible light polymerized gelatin hydrogels for 3D culture of hepatic progenitor cells*. Journal of Applied Polymer Science, 2016. **134**(11).



38. Bartnikowski, M., et al., *Protective effects of reactive functional groups on chondrocytes in photocrosslinkable hydrogel systems*. *Acta Biomater*, 2015. **27**: p. 66-76.
39. Somruethai, C. and T. Siriporn, *The Curing Efficiency and Mechanical Properties of Light-Activated Acrylic Resin*. *Macromolecular Symposia*, 2008. **264**(1): p. 140-143.
40. Truong, V.X., et al., *Red Light Activation of Tetrazine–Norbornene Conjugation for Bioorthogonal Polymer Cross-Linking across Tissue*. *Chemistry of Materials*, 2017. **29**(8): p. 3678-3685.
41. Fenn, S.L. and R.A. Oldinski, *Visible light crosslinking of methacrylated hyaluronan hydrogels for injectable tissue repair*. *J Biomed Mater Res B Appl Biomater*, 2016. **104**(6): p. 1229-36.
42. Xiao, P., et al., *Visible light sensitive photoinitiating systems: Recent progress in cationic and radical photopolymerization reactions under soft conditions*. *Progress in Polymer Science*, 2015. **41**: p. 32-66.
43. Shnitkind, E., et al., *Anti-inflammatory properties of narrow-band blue light*. *J Drugs Dermatol*, 2006. **5**(7): p. 605-10.
44. Zhang, Y., et al., *Antimicrobial Blue Light Therapy for Multidrug-Resistant *Acinetobacter baumannii* Infection in a Mouse Burn Model: Implications for Prophylaxis and Treatment of Combat-related Wound Infections*. *The Journal of Infectious Diseases*, 2014. **209**(12): p. 1963-1971.
45. Masson-Meyers, D.S., V.V. Bumah, and C.S. Enwemeka, *Blue light does not impair wound healing in vitro*. *J Photochem Photobiol B*, 2016. **160**: p. 53-60.
46. Dai, T., et al., *Blue Light Rescues Mice from Potentially Fatal *Pseudomonas aeruginosa* Burn Infection: Efficacy, Safety, and Mechanism of Action*. *Antimicrobial Agents and Chemotherapy*, 2013. **57**(3): p. 1238-1245.
47. Anderson, D.G., et al., *A Combinatorial Library of Photocrosslinkable and Degradable Materials*. *Advanced Materials*, 2006. **18**(19): p. 2614-2618.
48. Hawkins, A.M., D.A. Puleo, and J.Z. Hilt, *Effect of macromer synthesis time on the properties of the resulting poly( $\beta$ -amino ester) degradable hydrogel*. *Journal of Applied Polymer Science*, 2011. **122**(2): p. 1420-1426.
49. Hawkins, A.M., et al., *Synthesis and analysis of degradation, mechanical and toxicity properties of poly(beta-amino ester) degradable hydrogels*. *Acta Biomater*, 2011. **7**(5): p. 1956-64.
50. Gong, J.-H., et al., *Biocompatible fluorinated poly( $\beta$ -amino ester)s for safe and efficient gene therapy*. *International Journal of Pharmaceutics*, 2018. **535**(1): p. 180-193.
51. Keeney, M., et al., *Development of Poly ( $\beta$ -amino esters)-Based Biodegradable Nanoparticles for Non-Viral Delivery of Minicircle DNA*. *ACS nano*, 2013. **7**(8): p. 7241-7250.
52. Brey, D.M., I. Erickson, and J.A. Burdick, *Influence of macromer molecular weight and chemistry on poly( $\beta$ -amino ester) network properties and initial cell interactions*. *Journal of Biomedical Materials Research Part A*, 2008. **85A**(3): p. 731-741.
53. Agrawal, C.M. and R.B. Ray, *Biodegradable polymeric scaffolds for musculoskeletal tissue engineering*. *Journal of Biomedical Materials Research*, 2001. **55**(2): p. 141-150.

54. Grounds, M.D., *The need to more precisely define aspects of skeletal muscle regeneration*. The International Journal of Biochemistry & Cell Biology, 2014. **56**: p. 56-65.
55. Discher, D.E., P. Janmey, and Y.-l. Wang, *Tissue Cells Feel and Respond to the Stiffness of Their Substrate*. Science, 2005. **310**(5751): p. 1139-1143.
56. Woo, S.L.-Y. and J.A. Buckwalter, *Injury and repair of the musculoskeletal soft tissues. Savannah, Georgia, June 18–20, 1987*. Journal of Orthopaedic Research, 1988. **6**(6): p. 907-931.
57. Collinsworth, A.M., et al., *Apparent elastic modulus and hysteresis of skeletal muscle cells throughout differentiation*. American Journal of Physiology-Cell Physiology, 2002. **283**(4): p. C1219-C1227.
58. Leipzig, N.D. and M.S. Shoichet, *The effect of substrate stiffness on adult neural stem cell behavior*. Biomaterials, 2009. **30**(36): p. 6867-6878.
59. Kot, B.C.W., et al., *Elastic Modulus of Muscle and Tendon with Shear Wave Ultrasound Elastography: Variations with Different Technical Settings*. PLOS ONE, 2012. **7**(8): p. e44348.
60. Brey, D.M., I. Erickson, and J.A. Burdick, *Influence of Macromer Molecular Weight and Chemistry on Poly( $\beta$ -amino ester) Network Properties and Initial Cell Interactions*. Journal of biomedical materials research. Part A, 2008. **85**(3): p. 731-741.
61. Fedorovich, N.E., et al., *The effect of photopolymerization on stem cells embedded in hydrogels*. Biomaterials, 2009. **30**(3): p. 344-353.
62. Mironi-Harpaz, I., et al., *Photopolymerization of cell-encapsulating hydrogels: Crosslinking efficiency versus cytotoxicity*. Acta Biomaterialia, 2012. **8**(5): p. 1838-1848.
63. Shao, J., Y. Huang, and Q. Fan, *Visible light initiating systems for photopolymerization: status, development and challenges*. Polymer Chemistry, 2014. **5**(14): p. 4195-4210.
64. Shimojo, A.A., et al., *The crosslinking degree controls the mechanical, rheological, and swelling properties of hyaluronic acid microparticles*. J Biomed Mater Res A, 2015. **103**(2): p. 730-7.
65. Nielsen, L.E., *Cross-Linking—Effect on Physical Properties of Polymers*. Journal of Macromolecular Science, Part C, 1969. **3**(1): p. 69-103.
66. Gupta, N.V. and H.G. Shivakumar, *Investigation of Swelling Behavior and Mechanical Properties of a pH-Sensitive Superporous Hydrogel Composite*. Iranian Journal of Pharmaceutical Research : IJPR, 2012. **11**(2): p. 481-493.
67. Chern, J.-M., W.-F. Lee, and M.-Y. Hsieh, *Preparation and swelling characterization of poly (*n*-isopropylacrylamide)-based porous hydrogels*. Journal of Applied Polymer Science, 2004. **92**(6): p. 3651-3658.
68. Wang, K., *Roles of Polymer Crosslinking Density and Crystallinity in Regulating Surface Characteristics and Pre-osteoblastic MC3T3 Cell Behavior*. 2011.
69. Annabi, N., et al., *Controlling the Porosity and Microarchitecture of Hydrogels for Tissue Engineering*. Tissue Engineering. Part B, Reviews, 2010. **16**(4): p. 371-383.
70. Fisher, P.D., et al., *Improved small molecule drug release from in situ forming poly(lactic-co-glycolic acid) scaffolds incorporating poly( $\beta$ -amino ester) and*

- hydroxyapatite microparticles*. Journal of Biomaterials Science, Polymer Edition, 2014. **25**(11): p. 1174-1193.
71. Cho, S.-W., et al., *Therapeutic angiogenesis using genetically engineered human endothelial cells*. Journal of Controlled Release, 2012. **160**(3): p. 515-524.
  72. *Coating of Antibodies or Recombinant proteins to 96-well plate surface*. [PDF] 2018; Available from: <https://www.biomol.de/dateien/protocols/Ancell/Ancell--Coating-Procedure.pdf>.
  73. Sitterley, G., *Attachment and Matrix Factors*. Life Sciences Biofiles, 2008. **3**(8).
  74. Labarca, C. and K. Paigen, *A simple, rapid, and sensitive DNA assay procedure*. Anal Biochem, 1980. **102**(2): p. 344-52.

## VITA

### Place of Birth

- Edgewood, Kentucky

### Educational institutions attended and degrees already awarded

- Bachelors of Science, Physics  
Thomas More College, Crestview Hills  
Kentucky

### Professional positions held

- Research Assistant, Regenerative Biomaterials  
Laboratory, University of Kentucky, Lexington  
Kentucky
- Teaching Assistant, Department of Physics &  
Astronomy, University of Kentucky, Lexington  
Kentucky

### Scholastic and professional honors

- Outstanding Masters Student in Biomedical  
Engineering Award

### Professional publications

- Kohrs, N.J., et al., *Drug Delivery Systems and  
Controlled Release*, in *Reference Module in  
Biomedical Sciences*. 2018, Elsevier.

### Typed name of student on final copy

- Nicholas John Kohrs